POLITECNICO DI TORINO

Department of Mechanical and Aerospace Engineering
Master Degree in Mechanical Engineering

A.A. 2020/2021

Master of Science Thesis

Numerical simulation of adhesive joints under impact loading conditions

ADVISOR

Prof. Luca Goglio

CANDIDATE

Alessandro Tartaglione

CO-ADVISORS

Boursier Carlo Niutta
Ciardiello Raffaele
Fiumarella Dario

Contents

Abstract

Adhesive joining technology is now extensively used in different fields of application, in particular in the automotive industry thanks to its ability to exhibit a smooth stress distribution along the bonded area which is particularly useful for lightweight composite structural parts. However, there are limited standards or procedures generally adopted in research or industry to study the mechanical behaviour of adhesive joints subjected to impact. The thesis aims to propose and develop a LS-DYNA model to evaluate the mechanical properties of adhesive joints under impacts. The main aim of this work is to propose a model and a methodology that can assess the behaviour of the adhesive joints under impact loading and to validate it via experimental tests. The activity was carried out on composite and steel substrates bonded with an adhesive used in the automotive industry.

Chapter 1

Introduction

1.1 Adhesives for structural joints

Adhesive bonding is a joining technique in which the structural adhesive material creates a strong connection between two parts. Compared to the traditional joining techniques like welding, spot welding, riveting or bolts, adhesive joining usually provide a smoother stress distribution, higher fatigue resistance as well as high relative strength. Not to mention one of their main property that is the ability to join dissimilar materials and the compatibility with modern composite and lightweight materials. Despite their various advantages adhesive joints carry some complications if compared to traditional joining techniques both in design and production. For structural applications the bonding procedure needs to be carefully designed in order to obtain the rated mechanical properties; many external factors may affect the results: e.g. if a shear test is performed on a single-lap joint between two metal plates made under dry conditions, failure occurs in the adhesive layer, meaning that the adhesive force is larger than the cohesive one, fully exploiting the adhesive shear strength. The presence of water may affect the bonding force and the failure would occur at the interface reducing the strength of the joint. In any case, if properly designed and manufactured an adhesive joint is as reliable, or better, than a traditional joint.

Regarding the manufacturing process, the main steps to make an adhesive joint are [8]:

- surface cleaning;

- surface preparation;

- application of adhesive;

- closing the joint;

- curing.

Surface cleaning is necessary to remove any loose material, oil, or any contaminant that may affect the final joint integrity. Surface preparation includes the specific operations to be done depending on adherends and adhesive material, but also on the operating field of the component. Application of the adhesive may be performed manually or automatically and its crucial to deploy the right amount of it in the right position. Modern automatic layer deposition techniques (figure 1.1) make possible the implementation of manufacturing process and quality control. The final steps are the assembly of the joint and the curing process that is usually performed in autoclave to have the correct process parameters in terms of pressure and temperature. When pressure is not needed it can be done in a paint oven. Once the curing is complete, quality control and non destructive tests can be performed on the complete joint. By the way, this is still an open field of research. Despite some interesting modern inspection techniques like "ultrasound" or "acoustic emissions" tests, destructive tests (static, impact, fatigue) are nonetheless the most established ones.

In most cases, it cannot be done an effective adhesive joint by just substituting the traditional type of joining solution with adhesive layers; a specific design is required,
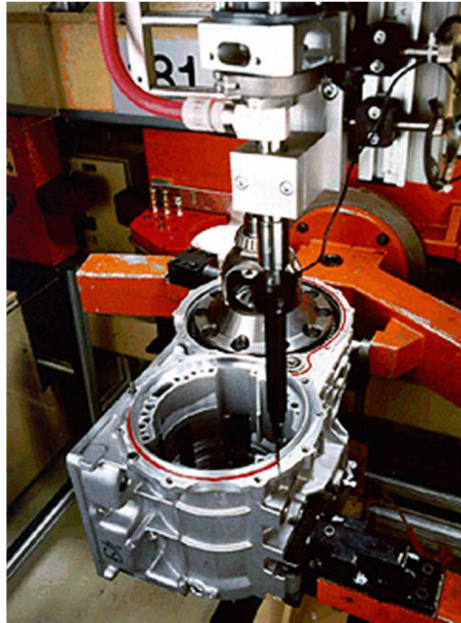
Figure 1.1: Automatic adhesive layer deposition in the automotive industry.

that takes into account the loading conditions in terms of loading distribution and type (static, fatigue, impact). The most established design methodologies require the following steps:

- Analysis of the stress distribution;

- Strength evaluation criteria;

- Optimization of the joint layout;

- Mechanical characterization of the adhesives;

- Methods for the joint quality control.

To properly evaluate the stress distribution, the loading condition have to be considered taking into account that adhesives exhibit different behaviour under different loads. E.g. they bear compression very well, most adhesives have better mechanical properties in shear than in tensile, they have poor strength in peeling due to the fact

that the stress is concentrated in a small area. To evaluate the static strength of
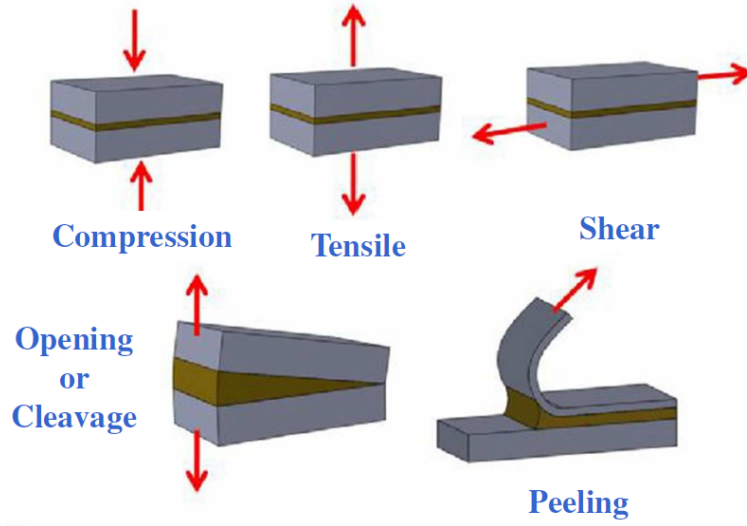

Figure 1.2: Typical loading conditions for adhesive joints.

adhesive materials a "mean stress" approach is not valuable due to the non uniform stress distribution exhibited by real joints (Fig.1.3). Better approaches are numerical modelling, which is discussed in section §1.5, or analytical models like *Bigwood Crocombe (BC)*. This model consider peel and shear stress constant through the thickness

Figure 1.3: Visual representation of the not uniform shear deformation of the adhesive in a SLJ with deformable adherends.

and variable along the overlap. The stress analysis of a shear test on a single lap joint like the one in Figure 1.3, according to the BC model, produces a higher stress close to the edges and a minimum in the center of the overlap (plot in Figure 1.4).
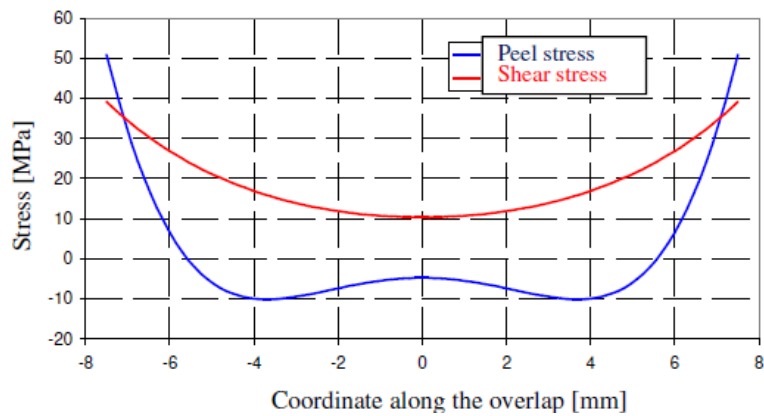
Figure 1.4: Peel and shear distribution according to the BC model in a single lap joint shear test.

Regarding the joint layouts the key rules that the designer has to remember are:

- To use the largest available joining area;

- To use the most favourable design configurations.

Nevertheless, this is still a wide field of research, there isn't a unique solution and the joint shapes and geometries can deeply differ case by case. Yet, there are some empirical rules that consistently produce better results, as can be seen in figure 1.5

Figure 1.5: Empirical rules for good adhesive joints design.

1.2 Adhesive materials

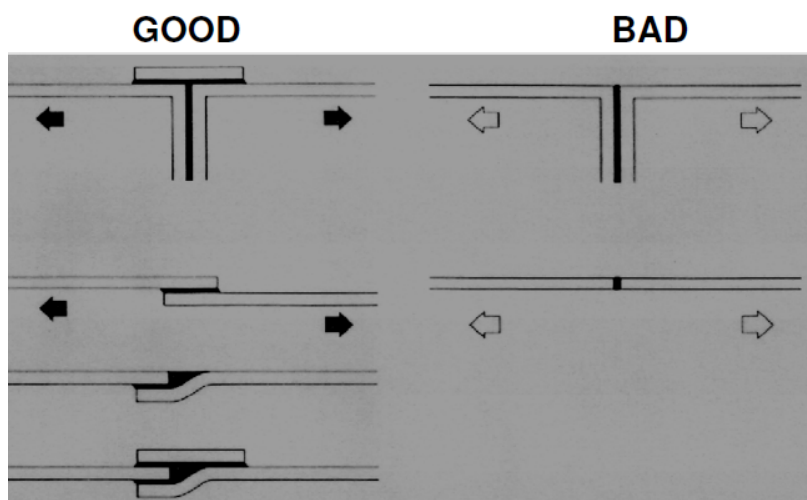A variety of adhesive materials are currently available in the industrial market. A classification of the main families of adhesives, based on the mechanical properties, is shown in figure 1.6. Focusing on polymers for structural adhesives the most widespread are epoxies and phenol-formaldehyde resins. Unfortunately, structural adhesives are usually proprietary formulations, while manufacturers only supply details of properties and methods of use. Nevertheless, this adhesives are often brittle after curing, and their properties are known to be improved by the addition of rubbery compounds, as well as in many cases two monomers are mixed so as to obtain better final properties with an hybrid polymer. Epoxies can be provided in the form of film, in a single-component paste or in a two-part liquid: resin and hardener. Two-component epoxies are not easy to handle on the production line and in particular do not lend themselves to automated operations [8]. on the contrary, single-component epoxies require a elevated curing temperature (typically for 15 min at 180 $°C$ or 5 min at 200 $°C$).
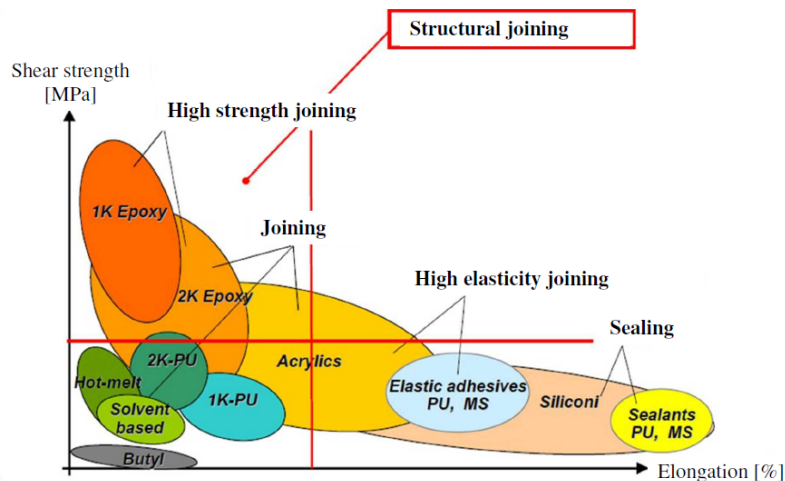

Figure 1.6: Adhesive materials classification.

Polyurethanes are an other class of structural adhesives commonly used in the industry e.g. for bonding windscreens in the automotive industry or large panels in coaches and caravans. They are available either as a two components or a single component that hardens through contact with atmospheric moisture. Polyurethane adhesives are subjected to loss in strength if prolonged exposed to moist, but this effect can be mitigated with the use of a primer. This class of adhesive is compatible with a variety of substrates: Composites including carbon fibre, FRP and GRP, metals, glass, wood and plastics. If compared to epoxy adhesives in terms of mechanical properties they exhibit lower strength and greater flexibility.

1.3 Adhesives and adhesive joints under impact loading

Impact behaviour of adhesive joints is a dynamic field of research nowadays, mainly due to the industrial interest of such joints and the widespread structural applications that they have. Applications in several industries, like automotive, aerospace, defence, and naval require that the products are able to adequately sustain impact loadings. As a consequence it's now necessary to study and optimize adhesive joints behaviour under this kind of loading, that is not straightforward because adhesives, like most polymer based materials, have a significant change in mechanical properties at different strain rates. Impact testing is in general a complex subject due to the high performance sensor and data logging sequence required; high strain rate conditions can be badly replicable, or, in some cases, a transition from ductile to brittle behaviour can produce unexpected results. Similarly to metallic materials, various polymers exhibit significant increase of modulus and ultimate stress at the cost of a reduction in the ultimate strain. But, differently from metallic material, this is

guided by the viscoelastic properties of polymeric materials. While the basic mechanical properties might increase, the reduction of elongation suggests a reduction in the fracture toughness due to a ductile-brittle transition. Some analytical models have been developed like *Cowper and Symonds (1957)* that defines a costitutive equation that adequately describe the phenomenon for the considered classes of materials. The work in [6] demonstrates the impact that strain rate has on fracture toughness, in which the fracture energy decreases as the strain rate increases. To quantify this sensitivity a 40% decay of fracture energy from the quasi static test to a test performed at 10 m/s has been registered.

Impact tests can be performed on bulk adhesives or on complete joints. The latter can be more complicated but is a closer approximation to the behaviour of real parts by taking into account adhesion and substrate properties and consequently has a bigger industrial interest. This family of tests is the one in which this work sits. Tests on bulk materials are still necessary to estimate the mechanical properties, like tensile and shear strength as well as fracture toughness, and are fundamentally used in material research. In this group can be highlighted tensile tests for tensile stiffness and strength [11]; for shear strength the Thick adherend Shear Test (TAST) [1] and the Notched plate shear method (Arcan) test [11]; for fracture toughness one of the most established test is the standardised double cantilever beam (DCB) [3].

Impact tests on adhesive joints are classified according to the chrosshead velocity:

- low velocity (up to 5 m/s)

- medium velocity (between 5 and 10 m/s)

- high velocity (between 10 and 100 m/s)

In the low velocity range are mainly used pendulum impact test machines like in the

Impact Wedge-peel test [2] or the Block Impact test [4]; in the high velocity range the Split Hopkinson Pressure Bar (SHPB) [7]; and in the medium velocity range are used drop dart testing machines, that is the machine for which the specimen developed in this work is designed.

1.4   Parameters that affect the impact test results

The behaviour of adhesive joints under impact loading is affected by a number of parameters, not only the material properties of the substrate and adhesive, but also joint geometry, loading type and environmental variables have to be considered to evaluate test results.

An important role is held by the compliance of the adherends that can strongly affect the energy dissipation of the joint. A further complication introduced by some composite material is that most resin matrix used in carbon and glass fibre composites are known to exhibit strain rate dependency in their mechanical properties. Beevers and Ellis in [5], showed that tests with ductile substrate bonded with a strong adhesive produced results in which the adherend material was the main parameter affecting the failure. It is clear that the tenacity of substrate and adhesive both have to be taken into account: a brittle adhesive is not able to plastically deform for example a ductile metallic substrate, drastically lowering the impact performance of the joint; and high strength adherends bonded with a tough adhesive is still unable significantly absorb energy. In general, the adhesive itself cannot provide a big contribution to the toughness of a joint, even in case of some epoxy structural adhesives that are modified with rubbery compounds or other flexibilisers that exploited improved energy absorption capabilities. But this is the condition that needs to be aimed whether the adhesive properties are the ones to be isolated.

Single lap joints are the most commonly used for impact tests on adhesive joints. Vaidya and Abhay in [12] studied the impact behaviour of SLJ under transverse impact loading with the specimen configuration show in figure 1.7. Carbon/epoxy
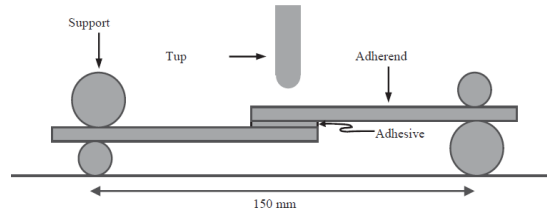

Figure 1.7: Scheme of the SLJ test setup [12].

composite adherends were used with an epoxy adhesive and were tested with a drop dart testing machine. The LS-Dyna analysis of this model revealed a non uniform stress distribution, with compression on the upper edge and tension on the lower one. The failure was mixed mode with predominant peel due to lower tensile properties of adhesives compared to compressive and shear ones.

The work in [9] studied a similar SLJ under in plane load insisted of transverse one. It was found out that the rupture initiates near the middle area along the width direction (on the bond-line) as a consequence of the uneven stress distribution, a difference of 13% was recorded between the centre and the border of the adhesive.

This work propose a double lap alternative that can be put in contrast with some of the researches previously made. In fact, this strapped lap, despite the uncertainty introduced by the double adhesive layer, produces a much more uniform stress distribution and makes possible to isolate the failure mode I, or with some alternative geometries, failure mode II.
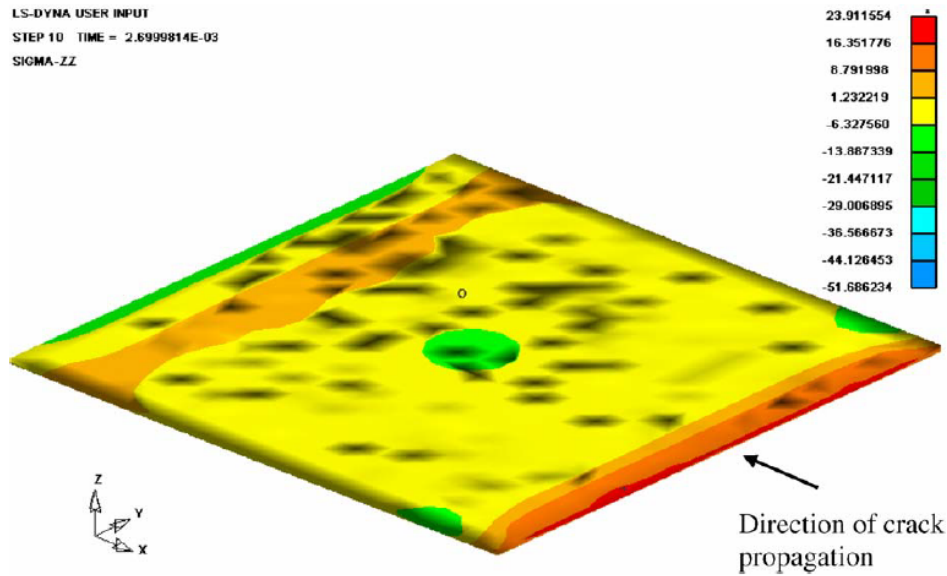
Figure 1.8: Peel stress distribution in the adhesive layer before crack nucleation. The units are in MPa [12].

1.5 Adhesives modelling with LS-DYNA

Modern numerical modelling solvers are an extremely useful instrument in design and validation of adhesive joints. As anticipated before, the stress inside the adhesive is strongly non uniform, as a consequence FEM analysis represents the best solution to predict the component behaviour with good approximation. Numerical modelling not only reduces the number of experimental and destructive tests required, it also gives some added value to them; for instance the stress-strain distribution and concentration of an impact test can be studied, giving details on material and component behaviour that are difficult to obtain via experimental tests or theoretical approaches.

There are two approaches currently used to model adhesives: one consists in the implementation of a mesoscopic model that incorporates stress-strain relationships, strain rate and pressure sensitivity and softening effects mostly used to calibrate the

models used in large scale analysis. The second approach describes the adhesive layer using a cohesive zone model or a constraint defined by a traction separation law. This approach comes with a lower computational cost allowing a better implementation in large-scale analysis. Nowadays full car crash tests are extensively used in car manufacturing companies; adhesives joints are the state of the art in many relevant crash test components of a car as they overcome the weaknesses that high strength steel and composite material exhibit under the concentrated loads introduced by traditional joining techniques. Models that have application in the industry for Ls-Dyna include MAT_138, which is the chosen one for this work, and MAT_240. The latter implements a trilinear traction separation lay that includes strain rate sensitivity. One common problem in adhesive modelling is its mesh dependency; the spacial discretization of the connection has to be very fine compared to the element size usually used on components and full full car scale. Fem based on explicit time integration cause a decrease in time step or ar increase of added mass. On this aspect the use of *cohesive elements* constitutes an advantage, being the material law *stress-displacement*, the critical timestep is independent of element thickness. Moreover, zero thickness and null initial volume are admissible and density can be specified per unit area as well. Common alternatives based on volume elements and 3-d material models e.g. *MAT_ARUP_ADHESIVE (*MAT_169), are thickness sensitive and as it tends to zero, critical timestep tends to zero as well. With cohesive elements, being the material law displacement driven, the local (interface) stresses are computed from the local relative displacements at integration points and not from the local strain. As a consequence, the interface stiffness is not defined as a classical stiffness, but has the

units of $force/length^3$ or $stress/length$:

$$\begin{bmatrix} \sigma_1 \\ \sigma_2 \\ \sigma_3 \end{bmatrix} = \begin{bmatrix} E_t & 0 & 0 \\ 0 & E_t & 0 \\ 0 & 0 & E_n \end{bmatrix} \cdot \begin{bmatrix} \delta_1 \\ \delta_2 \\ \delta_3 \end{bmatrix} [N/mm^2] = [N/mm^3] \cdot [mm] \qquad (1.5.1)$$
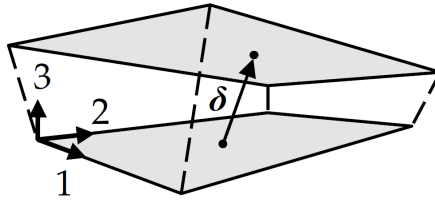

Figure 1.9: Cohesive elements principal direction scheme.

Cohesive elements material behaviour is defined in the normal and shear direction which is established by the thickness direction definition. This direction is fixed by the node numbering. Cohesive elements are attached to the substrates via coinincident nodes (merging nodes), or via tied contact. Two element formulations are available and their scheme is shown in figure 1.10:

- ELFORM = 19: moments are not transferred, suitable to tie volume elements;

- ELFORM = 20: moments are transferred, suitable to tie shell elements with offset ($moments = forces \cdot offset$).

1.5.1 MAT_138

MAT_138 is a simplified model that incorporates a triangular traction separation law. Despite its simplicity, if properly calibrated, it guarantees valuable results in particular with the epoxy structural adhesives that this work is focused on. The key material parameters are the peak traction and shear stress (T, S), the ultimate displacement at failure in the same directions (UND, UTD), the energy release rate in traction and
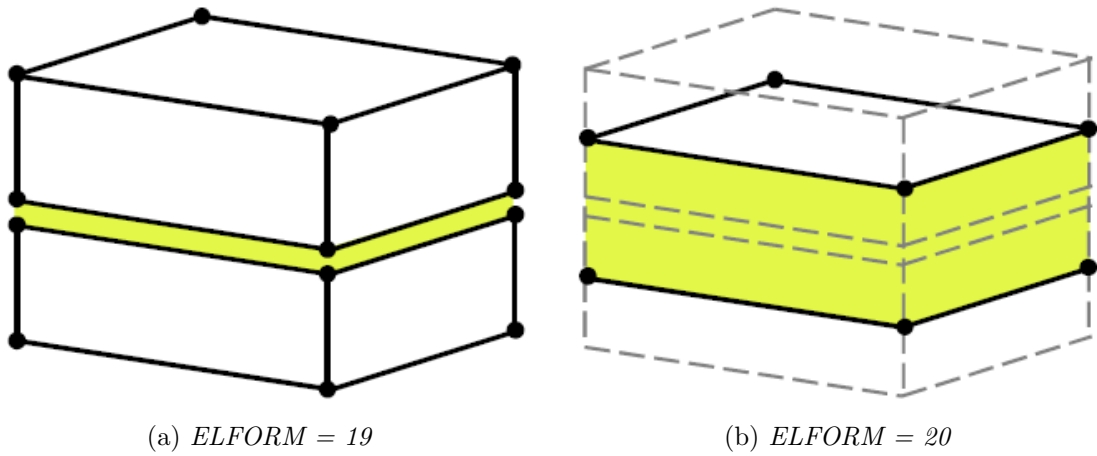
(a) *ELFORM = 19* (b) *ELFORM = 20*
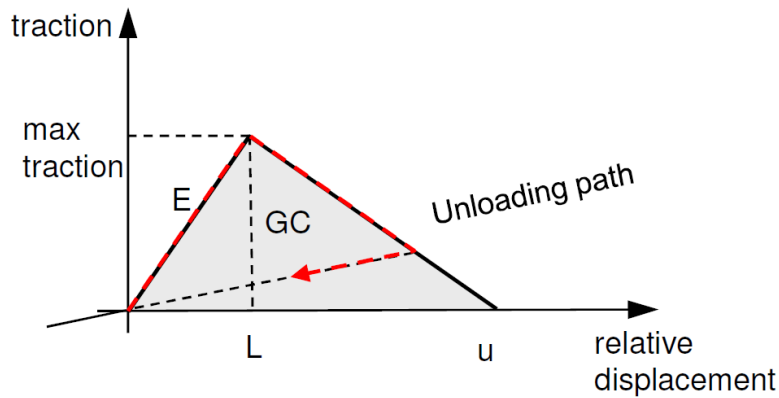
Figure 1.10: ELFORM 19 and 20 scheme.

Figure 1.11: MAT_138 traction separation law.

shear (GIC, GIIC) the mixed mode power law coefficient (XMU). It's a purely elastic cohesive zone model with damage and doesn't have plasticity. As shown in figure 1.11 damage of the interface is considered, that is, irreversible conditions are enforced with loading/unloading paths coming from/pointing to the origin.

Mat_138 includes a quadratic mixed mode delamination criterion and a damage formulation. The total mixed mode relative displacement δ_m is function of the peel
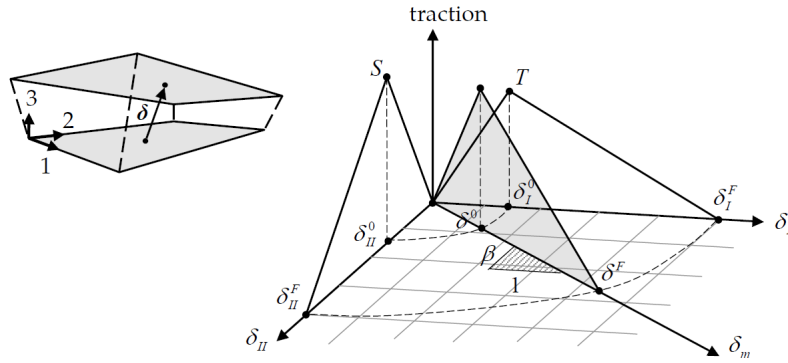
Figure 1.12: MAT_138 mixed mode characteristic.

and total shear displacement:

$$\delta_m = \sqrt{\delta_I^2 + \delta_{II}^2} \quad \text{with} \quad \begin{aligned} \delta_{II} &= \sqrt{\delta_1^2 + \delta_2^2} \\ \delta_I &= \delta_3 \end{aligned} \tag{1.5.2}$$

The mixed mode characteristic show in figure 1.12 is computed as a combination of the mode I and mode II separation law. The mixed mode *damage initiation displacement* δ_0 is function of the principal direction material properties and the load angle β and the *ultimate mixed mode displacement* is also function of the power law coefficient (XMU). The material model also include two error checks to ensure proper material data, or in particular that the damage initiation displacement is smaller than the ultimate displacement.

1.5.2 MAT_240

The material type 240 is a strain-rate dependent, elastic-ideally plastic cohesive zone model. It has a trilinear traction separation law which is defined in tension and in pure shear. It includes a quadratic yield and damage initiation criterion in mixed mode and the damage evolution is governed by a power law formulation. The model is suitable only for cohesive element formulations (ELFORM 19-20). The material properties are specified for mode I and mode II; the main parameters are:

- ρ: mass density;

- T,S: yield stress in mode I and mode II;

- EMOD, GMOD: Young's modulus in mode I and mode II;

- THICK: Cohesive thickness;

- GIC_0, GIIC_0: energy release rate in mode I and mode II;

- FG1, FG2: parameter that describes the tri-linear shape of the traction separa-
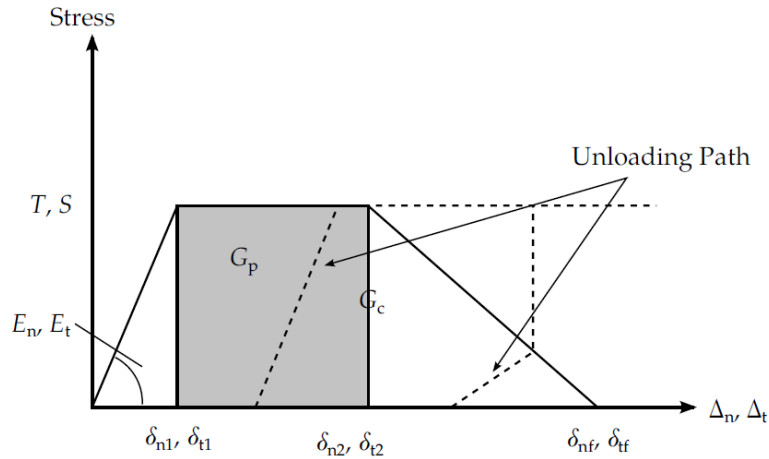 tion law in mode I and mode II.

Figure 1.13: MAT_240 trilinear traction separation law.

The traction separation law is described in figure 1.13. It has to be remarked that the initial stiffness (E_n, E_t) in both modes are calculated from the elastic Young's and shear moduli respectively:

$$E_n = \frac{EMOD}{THICK}$$
$$E_T = \frac{GMOD}{THICK}$$

(1.5.3)

The shape parameter *fg*, on the contrary of MAT_138, is necessary to define the fixed shape of the traction-separation law in both modes and is equal to the ratio of the area under the constant stress (plateau) region and the energy release rate:

$$f_{g1} = \frac{G_{I,p}}{G_{IC}}$$
$$f_{g2} = \frac{G_{II,p}}{G_{IIC}} \tag{1.5.4}$$

This material model can account for strain rate effect. The dedicated parameters, if activated, can be set to obtain an increase in maximum stress and a reduction of fracture energy. For yield stress two rate dependent formulations are implemented: a *quadratic logarithmic* and a *linear logarithmic* function. The strain rate parameters can be independently activated and modulated for strength and energy. The equivalent strain rate $\dot{\varepsilon}_{eq}$ is evaluated by:

$$\dot{\varepsilon}_{eq} = \frac{\sqrt{\dot{u}_n^2 + \dot{u}_{t1}^2 + \dot{u}_{t2}^2}}{THICK} \tag{1.5.5}$$

Here $\dot{u}_n$, $\dot{u}_{t1}$, $\dot{u}_{t2}$ are the velocities corresponding to the three principal directions. $\dot{\varepsilon}_{eq}$ is evaluated at yield initiation, as a consequence the elastic region won't be affected by strain rate and the rest of the separation law will be function of this threshold value.

Chapter 2

Material and Methods

2.1 Impact test setup

This work investigated the possible implementation of an innovative impact test setup for adhesive joints. The specimen have been designed as a *single strap lap joint* to be tested with a standard drop dart testing machine. The solution proposed is aimed to be easily applicable with a variety of materials and could lead to a further development in material research regarding adhesive joints under large strain rate loading conditions, as well as a faster and safer design of impact sensible components in a variety of industry fields. The proposed geometry is shown in figure 2.1, as it will be further discussed, the specimen have been designed in order to obtain a failure mode I, while some variations of the same joint can be designed for the study of mode II or mixed mode.

The added value of a test like this is the study of a complete joint behaviour but still focused on adhesive material properties rather than the substrate ones. If compared to the established tests on bulk material, testing a complete joint makes possible to evaluate not only the cohesive properties, but also the adhesive ones, as well as the effect produced by the coupling of adhesive and substrate. Being the test designed for a drop dart testing machine, it sits in the low-medium velocity impact
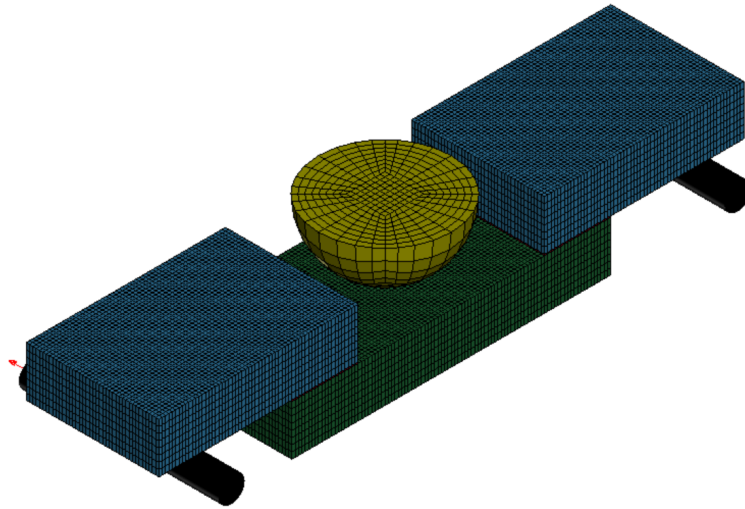
Figure 2.1: Joint geometry.

tests category and it can't be compared with higher strain rate tests like the SHPB.

The research started with numerical modelling in LS-DYNA with the objective to be validated and calibrated via experimental tests. Numerical modelling is a necessary step in this development for two main reasons: it makes possible to simulate a large number of tests with a low cost, at the same time it makes possible to deeply study the stress-strain field with decent accuracy accelerating a lot the geometry optimization to obtain the desired objectives. One of the main virtues of this work is its versatility: the key quotes of the joint are suggested to the tester in a parametrised and is easy to calculate as function of the main material properties, in order to obtain replicable results with a variety of materials, adhesives and substrates, for the desired failure mode.

2.2 Finite element modelling with LS-DYNA

The first step in this work has been to create the model in a completely parametrised way in order to be able to quickly tune its key parameters (mesh size, dimensions,

material properties, boundary conditions, impact parameters), overcoming the mesh generation, and model setup limits in the Ls-Dyna keyword editor Ls-prepost. This has been accomplished with a python script that operating the chosen mesh generator (cf. `https://gmsh.info/`), creates the joint component's mesh and assembles it in a keyword file together with all the necessary keywords for the model and post analysis.

Before going through the details of the model, the consistent measurement system chosen for all the performed simulations is remarked below:

- Length: mm;

- Weight: ton;

- Time: s;

- Force: N;

- Stress: MPa;

- Energy: mJ.

The test took care of the industry's most commonly used LS-DYNA formulations. While this could lead to a lower accuracy for material research, it helps to properly tune the models for large-scale analysis that needs to keep the computational cost as low as possible.

2.2.1 Adherends materials

The adherends have been initially modelled with shell elements. This choice given many advantages: first of all it's a suitable element formulation for the substrates

geometry, at the same time it helps keeping low the computational cost of the simulation, while being very compatible with composite materials that are commonly modelled in this way.

Two material models have been adopted for the substrates:

- *MAT_003/*MAT_PLASTIC_KINEMATIC;

- *MAT_058/*MAT_LAMINATED_COMPOSITE_FABRIC.

For metallic and composite materials respectively. *MAT_003 is a material model for isotropic and kinematic hardening plasticity. It's a very cost efficient model that is suitable for the studied specimen in which the deformation of adherends is very limited and plastic strain has to be avoided. In the concrete, the simplified model approximates the plastic region with a tangent modulus E_{tan} that is defined between yielding and ultimate tensile strain. The material studied is the *DD11 steel*: a hot rolled steel for plastic deformation usually used for deep drawing. It has a low yield strength and very good formability. The stress strain relationship in a tensile test according to the LS-DYNA material model is shown in figure 2.2, while the details on material properties are in table 2.1. Only kinematic hardening have been considered.

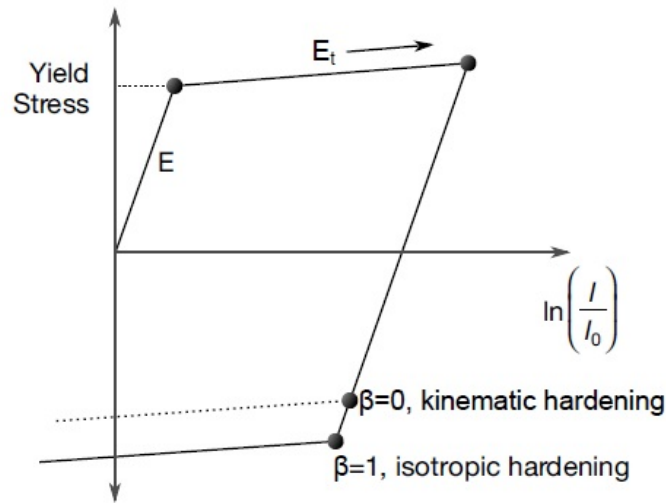| *MAT_003	
$\rho[Ton/m^3]$	7.8
$E[MPa]$	$200 \cdot 10^3$
$\nu[-]$	0.3
$\sigma_y[MPa]$	170
$E_{tan}[MPa]$	821.5
$\varepsilon_f[-]$	28%

Table 2.1: *MAT_003 material card for DD11 steel.

Figure 2.2: *MAT_003 material model.

*MAT_058/*MAT_LAMINATED_COMPOSITE_FABRIC* is the material card se-
lected for the CFRP simulation with shell. This model is suitable for unidirectional
composite layers, complete laminates and woven fabrics. In this work it was applied
to simulate a *carbon fibre composite laminate with epoxy matrix.* This material was
used in the experimental tests, the specimen were 20mm wide and 7.04 mm thick with
8 layers with 0/90 stacking sequence. The main mechanical properties are reported
in table 2.2.

Each part has been modelled with one shell, the layers and the stacking sequence
were defined with *PART_COMPOSITE producing one integration point for each
layer. With this schematization delamination cannot be modelled, but it's not an
expected event being the test designed to get an adhesive failure. MAT_58 imple-
mented a *modified Hashin* failure criteria and has been selected the option $FS = 1$: a
smooth failure surface with quadratic failure criteria for both the fiber and transverse
directions that is the suggested option for complete laminates and fabrics. Consid-
ered the simple specimen geometry, material axes have been defined with the option

*MAT_58	
$\rho[Ton/m^3]$	1.5
$E_a[MPa]$	$54 \cdot 10^3$
$E_b[MPa]$	$54 \cdot 10^3$
$\nu[-]$	0.08
$G_{ab}[MPa]$	3500
$\varepsilon_{1c}[-]$	0.0075
$\varepsilon_{1t}[-]$	0.0095
$\varepsilon_{2c}[-]$	0.0075
$\varepsilon_{2t}[-]$	0.0095
$\varepsilon_s[-]$	0.0296
$\sigma_{1c}[MPa]$	520
$\sigma_{1t}[MPa]$	800
$\sigma_{2c}[MPa]$	520
$\sigma_{2t}[MPa]$	800
$\sigma_s[MPa]$	84

Table 2.2: *MAT_58 material card for DD11 steel.

$AOPT = 2$, i.e. globally orthotropic with material axis that are defined with the vector $a = (1, 0, 0)$ that defines the longitudinal direction.

The shell element formulation has been suitable only for some of the tests performed. As further discussed in the geometry optimization section §2.2.4, many joint configurations require a quite significant substrate thickness. In particular if low strength materials are bonded with a wide overlap, that is the case of the DD11 steel. In case the thickness is not small if compared to the part width and length, the shell element formulation is known to not be accurate enough. In fact, the assumption of constant stress through the thickness direction which is normally acceptable with thin parts, in case of thicker ones introduces non negligible errors, making the specimen

result stiffer than it should be. Moreover, the tied contact commonly utilized to join the cohesive elements to the respective substrate nodes only works up to a limited offset, which is the distance between the cohesive nodes, and the substrate segment. In other words, if the thickness of the shell is big if compared to the mesh size, Ls-Dyna is not able any more to properly apply the tied contact.

For this reasons a model based on solid elements formulation for the substrates has been created. Element formulation 1 was selected for the isotropic and composite material both. This is the *constant stress solid elements* formulation; for stability purpose, in case of bending loading condition *hourglass energy* has to be activated in Ls-Dyna, and it has been limited to 5% not to affect much the results.

Regarding the material models, the DD11 material card *MAT_003 is suitable for shell and solid elements both. Moreover, no modification or further analysis was needed being this material isotropic, i.e. it exhibits the same properties in the three principal directions. The implementation of the solid elements formulation for the composite material was more complex. The selected material card for this purpose was the *MAT_59 COMPOSITE FAILURE SOLID. This implementation was difficult without the support of a dedicated material characterization. As a matter of facts, most laminate and composite fabrics suppliers only provide the typical in-plane material properties for their products. In laminates subjected to load in the transverse direction orthogonal to the fibres it's only the matrix that can bear the load. As a consequence, in this work they have been initially set to the average mechanical properties of the matrix (epoxy resin).

2.2.2 Adhesive materials

The adhesive has been modelled with a *cohesive zone model (CZM)*; the material model chosen is MAT_138, that, despite its simplified bilinear characteristic, is known to produce effective results with epoxy and other structural adhesive of interest of a test like this, anyhow the main characteristics of this keyword have already been explicated in section 1.5. A further development in this aspect would be the implementation of a more complex material model like MAT_240, that also has the possibility to study the strain rate sensitivity of the adhesive material.

The research has been focused on two materials, whose cards are shown in table 2.3, we are looking at a polyurethane and an epoxy adhesive. In particular the material properties of the epoxide have been chosen starting from experimental data of tests performed via the *Arcan test* in tensile, shear and 30, 45, 60 degrees loading condition. The data have been interpolated with the *_MAT_138 bilinear characteristic and further corrected via an LS-DYNA numerical simulation of the same test. Last remark on the adhesive modelling is the chosen contact keyword that is: *TIED_SHELL_EDGE_TO_SURFACE_CONSTRAINED_OFFSET*, that is suitable for cohesive elements, it can transmit forces and moments and thanks to the offset parameter a distance equal to half of the shell thickness can be set as fixed distance between adhesive and adherend coupled nodes. On the other hand, with the solid element formulation no tied contact has been defined; the coupled nodes have been merged.

*MAT_138 polyurethane		*MAT_138 epoxy	
$\rho[Ton/m^3]$	0.98	$\rho[Ton/m^3]$	1.22
$E_n[MPa]$	3.334	$E_n[MPa]$	8.0801
$E_t[MPa]$	3.334	$E_t[MPa]$	13.8175
GIC$[MPa \cdot mm]$	4.75	GIC$[MPa \cdot mm]$	3.4159
GIIC$[MPa \cdot mm]$	19.0	GIIC$[MPa \cdot mm]$	8.164
$\sigma_t[MPa]$	5.0	$\sigma_t[MPa]$	7.1913
$\sigma_s[MPa]$	10.0	$\sigma_s[MPa]$	13.9556
UND[mm]	1.9	UND[mm]	0.95
UTD[mm]	3.8	UTD [mm]	1.17
XMU[-]	2	XMU [-]	1

Table 2.3: *MAT_138 material card for epoxy adhesive (Right) and PU adhesive (Left).

2.2.3 BC, impactor modelling and control variables

The boundary conditions consists in a set of clamped nodes and a cylindrical rigid wall for each clamping side. This is the schematization chosen for the clamping system of the impact test machine. The rigid walls have been placed in order to evaluate whether the radius of curvature of the fillet of the clamping base has any effect on the results.

The impacting energy is provided by an hemispherical rigid body (Fig. 2.3). The impact velocity is set by an initial velocity condition, while the impacting mass is set with a calibrated density. This body is constrained in every degree of freedom except from the z (vertical) direction. This is a good schematisation of the dart that affects as little as possible the computational cost of the simulation. It can be noted that the rigid material may make the impact harsher, but actually it can be assumed that the machine is much stiffer than the tested specimen making this simplification acceptable.

The necessary termination time is usually about 0.5ms, while as control and post
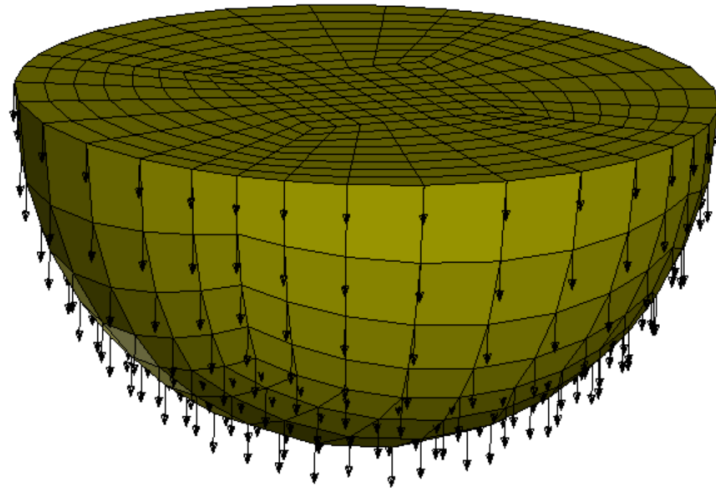
Figure 2.3: Impactor mesh with the assigned initial velocity to each node.

analysis optional variables have been set the following keywords:

- CONTROL_CONTACT;

- CONTROL_HOURGLASS;

- CONTROL_TIMESTEP;

- DATABASE_ASCII_OPTION;

- DATABASE_BINARY_D3PLOT;

- DATABASE_EXTENT_BINARY;

In DATABASE_BINARY_D3PLOT it was important to properly adjust the timestep according to the test duration or velocity so that the data were recorded with consistent resolution. The same remark is valid for the additional data saved in the *binout* with DATABASE_ASCII_OPTION. DATABASE_EXTENT_BINARY was used to add the material history variables and the elements strain tensor.

2.2.4 Geometry optimization

The aim of the test is to obtain the failure in the adhesive layer by tensile stress. It can be observed that the adhesive would bear pure tensile stress only with infinite stiffness of the adherends. In this hypothetical case the test would result in a rigid vertical translation of the bottom adherend while the top ones remain fixed stretching the adhesive only in the peel direction. On the other hand, the real joint bends under the load and it's this deflection that creates some axial forces that are transmitted through the adhesive. The higher the joint deflection is, the higher is the shear stress and deformation in the cohesive elements. A visual representation of this effect is shown in figure 2.4. The proposed comparison is between two equal configurations for material and geometry, except for the overlap. It can be seen that a higher overlap induces increased forces to detach the adherends and, consequently, causes a higher deformation. In this example, the higher shear deformation of the adhesive is clearly visible in the most bent joint. The solution to this problem has been to *define a specimen that is stiff enough to achieve an acceptable stress distribution in the adhesive layer*. To do so the specimen dimensions have been defined in order to maximize its stiffness.

Starting from the *adherends length*, apparently, increasing too much the top adherends overhang, or the bottom one length, makes its deflection much larger decreasing the overall joint stiffness. To prove this effect, an analysis on a joint with the following characteristics is here reported:

- Adherends material: DD11 steel;

- Adherends thickness: 2.1 mm;

- Adhesive material: Polyurethane;

(a) *8 mm overlap*

(b) *4 mm overlap*
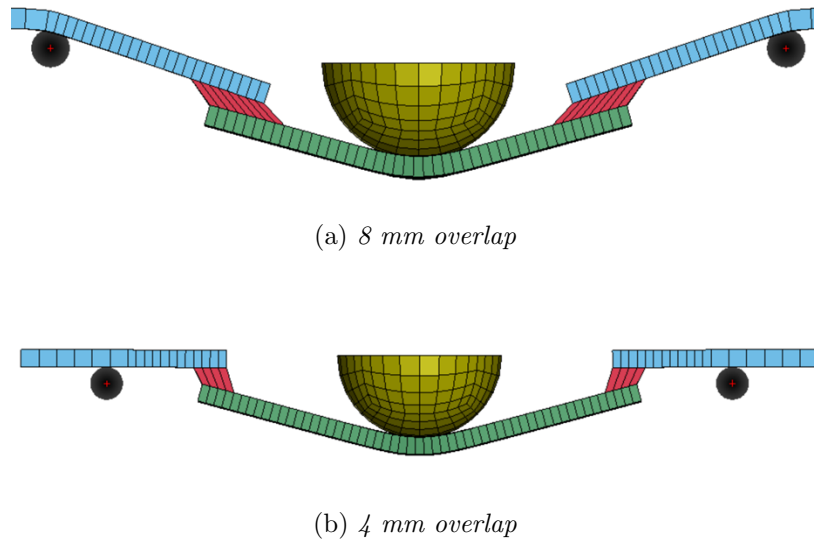
Figure 2.4: Visual representation of the effect of the adherends deformation on shear deformation of the adhesive.

- Ovelap: 3 mm.

It can be observed that the two extreme conditions in terms of substrates length: the bottom adherend as wide as possible (Fig. 2.5) and the bottom adherend as narrow as possible (Fig. 2.6) to let the 20mm gap in the middle for the impactor, are subjected to a large deformation of the longest adherend. The intermediate solution (Fig. 2.7) distributes the strain better between the components minimizing the shear stress stand by the adhesive material as shown in the shear and peel stress plots in figure 2.8. The wide and narrow specimen has the shear component which is the predominant one; the average one has certainly the better stress distribution, despite being still not enough as the shear component is not negligible and the failure can be considered for mixed mode. The best solution to further reduce the shear stress would be to increase the substrate thickness as will be discussed in section 2.2.5.

This result is reasonable also considered that a beam bending stiffness is inversely proportional to the cube of its length, so the optimum could only have been in the

(a) *Undeformed.*

(b) *Deformed.*
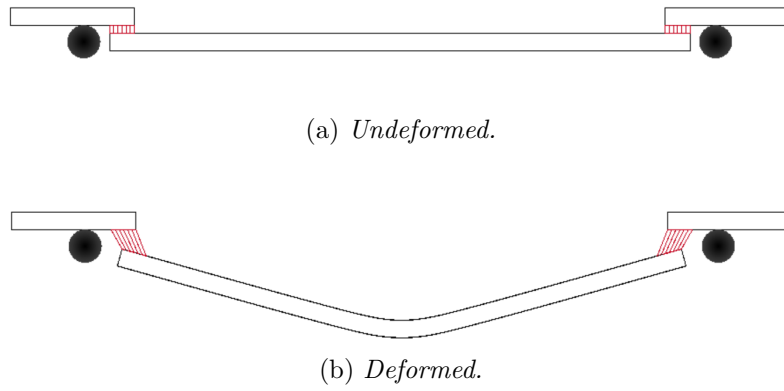
Figure 2.5: Joint configuration with the bottom adherend as wide as possible.

(a) *Undeformed.*

(b) *Deformed.*
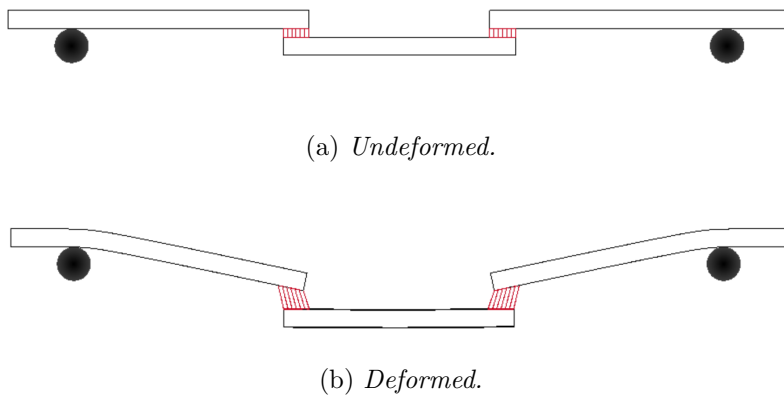
Figure 2.6: Joint configuration with the bottom adherend as narrow as possible.
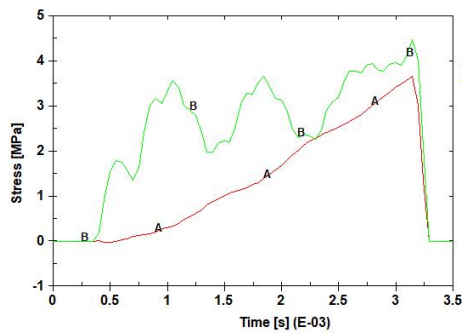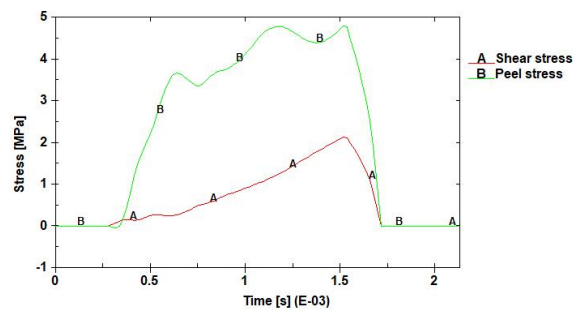

(a) *Undeformed.*

(b) *Deformed.*
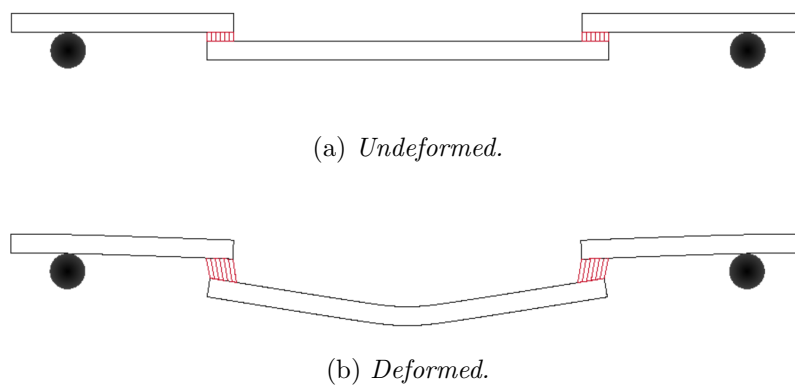
Figure 2.7: Joint configuration with the bottom adherend at an average length.
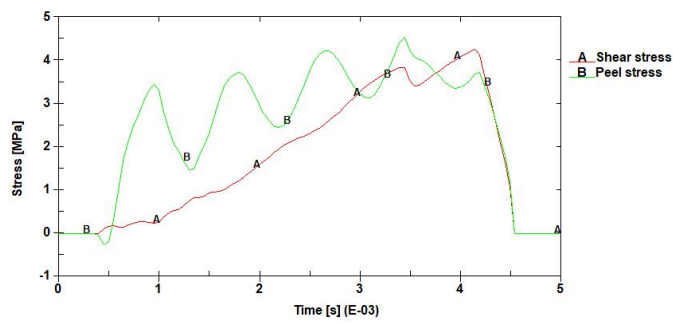
(a) *Wide joint*

(b) *narrow joint.*

(c) *average joint.*

Figure 2.8: Peel and shear adhesive stress for the three geometries.

middle. As a consequence, the adherends length has been set so that the center of the overlap is at half distance between the impactor and the support. Considering the 76.2 mm span of the drop dart testing machine clamping system, the best results have been obtained with a distance from the support to the adhesive center of 19mm-20mm, at least as long as the overlap is small enough. In fact, getting closer to the maximum overlap length achievable it's not possible to strictly follow this condition because a space between the two top adherends equal to the dart diameter (20mm) has to be left open.

The specimen width doesn't really affect the test from a theoretical point of view. Seeing the adherends as beams it is known that the bending stiffness is proportional to the area moment of inertia of the cross-section and the moment of inertia is linearly proportional to the width (for a rectangular cross-section). At the same time the adhesive strength is proportional to its bonding area and so it linear too with the width. In reality a small deviation could be noticeable due to the different relative strength that adhesive materials exhibit with variable bonding surface, but, more importantly, the circular clamping system of the machine doesn't allow to increase too much this quantity. In conclusion the specimen width have been fixed to 20mm.

An alternative presented is a joint with the bottom adherend wider than the ones on the top. E.g. the joint shown in figure 2.9 that resembles the 2.1mm adhesive, 3mm overlap test studied before, with a bottom adherend width increased to 30 mm. In this case the force necessary to make the adhesive fail is the same, but the bottom adherend is stiffer than before thanks to the increased moment of inertia. The result is an overall stiffer joint and a minimized shear stress in the adhesive if compared to the optimal solution of the plot in figure 2.8 (c). As clearly shown in this example, the previous test with this modification can exhibit a failure mode I, proving how

this solution is valuable whether it's not possible to further increase the adherends thickness.

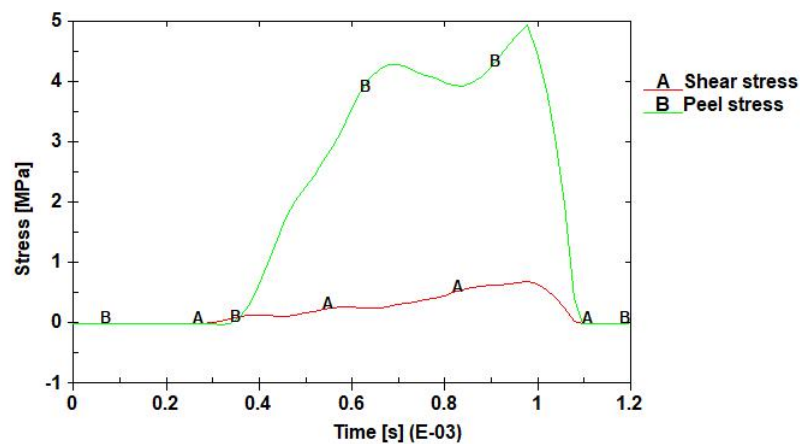Figure 2.9: Bottom adherend wide geometry.

Figure 2.10: bottom adherend wide stress.

2.2.5   Adherends thickness: analytical approach

The last and most important dimension to define is the adherend thickness. Clearly for this parameter an optimum doesn't exist, on the contrary, increasing it strongly increase the overall specimen bending stiffness. For this reason the adherend thickness has been chosen as the changing dimension as a function of the overlap length and material properties. This test aim to be versatile with a variety of materials, and

also the overlap length needed to be a changeable variable for the tester, as long as it is limited to a reasonable value. To accomplish this requirement a quick and parametrised estimation of the required thickness is needed; to do so, an analytical approach has been adopted.

The relatively simple geometry of the specimen made possible an approximated analysis with the beam theory. In fact, isolating one of the two top adherends and drawing the free body diagram of the latter, it can be seen as an Euler-Bernoulli cantilever bream loaded near the tip (at the center of the adhesive) as shown in figure 2.11.
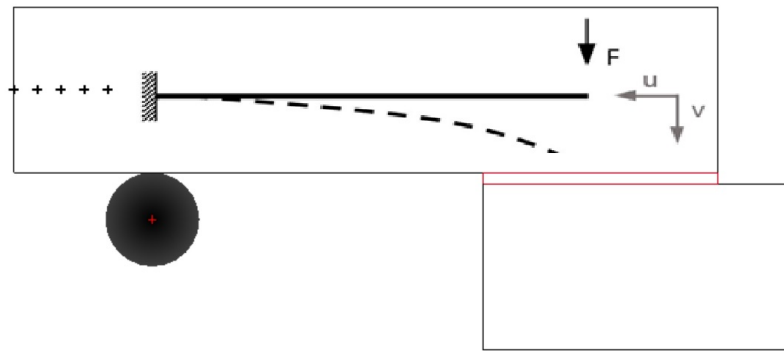
Figure 2.11: Cantilever beam model.

On an edge the adherend is clamped and the load is transmitted by the adhesive layer, whose maximum force is the adhesive strength multiplied by the surface area of adhesive in that particular configuration. The main hypothesis in this approach are:

- Small deflections;

- Thin beam;

- Concentrated load;

- Static loading condition.

The bending stiffness of a cantilever beam is:

$$K = \frac{F}{\delta} = \frac{3EI}{l^3} \tag{2.2.1}$$

with

$$F = \sigma_a \cdot Ovl$$
$$I = \frac{bh^3}{12} \tag{2.2.2}$$

In which σ_a is the adhesive tensile strength in MPa and Ovl is the adhesive overlap in mm. It can be seen that fixing an acceptable displacement δ the thickness h of the adherends that predict that chosen displacement at distance l from the clamping can be computed. The LS-DYNA simulations shown that regardless the joint configuration a displacement of 0.05 mm at $l = 20$ mm produces a shear stress of about 1% of the shear strength of the adhesive and a peel stress greater than 99% of the tensile stress. In this condition the mixed mode component is negligible and the failure mode is like failure mode I.

After substituting for the force F, the area moment of inertia I and solving for the thickness h the following relationship is obtained:

$$h > \sqrt[3]{\frac{640\sigma_a \cdot Ovl}{E}} \tag{2.2.3}$$

In which E is the adherend young modulus in GPa. It can be noted that the specimen width b doesn't affect the test.

Obviously, if plasticity in the substrates occurs, this elastic model is not valid any more, so a second condition has been set with the same approach. Starting from the maximum stress in the same cantilever beam $\sigma = M/W$, with $W = bh^2/6$, the following relationship is obtained:

$$h > \sqrt{\frac{120\sigma_a \cdot Ovl}{\sigma_s}} \tag{2.2.4}$$

In which σ_s is the yield strength of the adherends.

An alternative proposed is to model the whole joint as a clamped-clamped beam loaded in the middle as shown in figure 2.12.
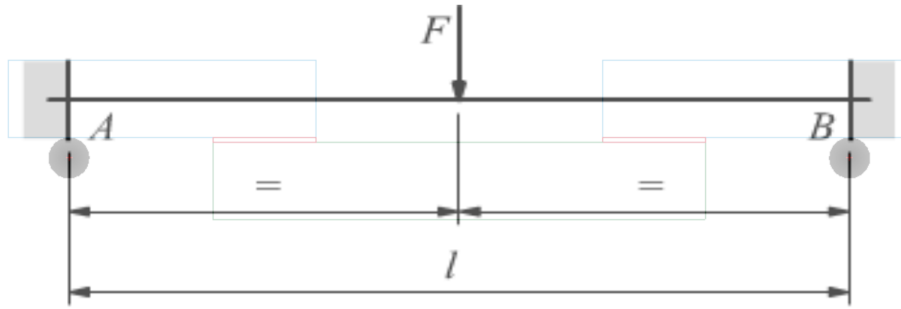

Figure 2.12: Clamped-beam model scheme

In this case the biggest simplification introduced is considering the specimen as a uniform beam, but actually the overlap produces a stiffening and at the same time the adhesive is compliant with the bending deformation and the two errors tends to compensate each other. In this second scheme the F.B. diagram suggests a load applied in the middle equal to the adhesive strength σ_a multiplied by the surface area of adhesive in both the joining regions, which means a load equal to the double of the one considered in the previous scheme. Being the relative length of the adherends fixed, the numerical simulation shown that the displacement $\delta = 0.05\ mm$ of the top adherends produces a proportional displacement of the bottom one of $0.08\ mm$. The absolute displacement of the centre of the joint is actually much larger than that, being strongly affected by the elongation of the adhesive as well as the localized deformation near the impact region. On the contrary this analysis aims to isolate the bending displacement of the substrates which is the one that induces shear in the adhesive. As a consequence, the displacement has been evaluated in a section far from the dart contact region and subtracted by the elongation of the adhesive.

The bending stiffness of a clamped-clamped beam is:

$$K = \frac{F}{\delta} = \frac{192EI}{l^3} \tag{2.2.5}$$

with

$$F = 2\sigma_a \cdot Ovl$$
$$I = \frac{bh^3}{12} \tag{2.2.6}$$

With the same approach used before the displacement of the bottom of the adherend have been fixed and the stiffness equation has been solved for the thickness h resulting in a relationship very similar to the one of the cantilever beam model:

$$h > \sqrt[3]{\frac{691.3\sigma_a \cdot Ovl}{E}} \tag{2.2.7}$$

In which it has been fixed $l = 76.2 \ mm$ that is the span of the drop dart machine clamping system. Similarly to the previous case, a condition on the yield stress has been set:

$$h > \sqrt{\frac{114\sigma_a \cdot Ovl}{\sigma_s}} \tag{2.2.8}$$

The two simplified models have been verified by comparing the displacement of the nodes of a section far from the impacting region at the moment of maximum bending deformation in the numerical simulation and the solution of the beam theory problem. For the cantilever beam loaded at a distance a = 20mm it is:

$$z = \frac{Fx^2}{6EI}(3a - x) \quad \text{for} \quad 0 < x < a$$
$$z = \frac{Fa^2}{6EI}(3x - a) \quad \text{for} \quad a < x < l \tag{2.2.9}$$

While for the clamped-clamped beam model it is:

$$z = \frac{F}{48EI}(4x^3 - 3l^2x) \quad \text{for} \quad 0 < x < l/2 \tag{2.2.10}$$

In figure 2.13 is shown the numerical-analytical comparison for a joint configuration that will be called *test A* whose geometry is shown in table 2.4. This is a
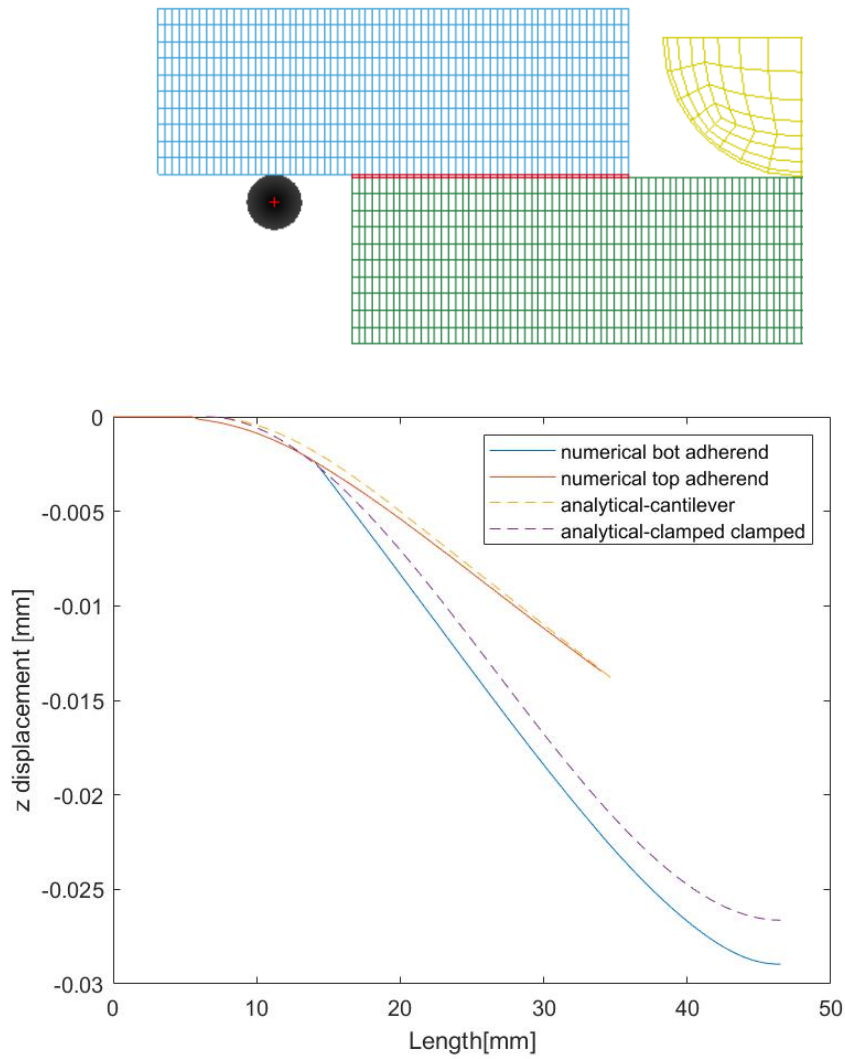
Figure 2.13: TEST with DD11 steel substrates, 12mm thickness, epoxy adhesive and 20mm of overlap. Comparison of the analytical solution of the two beam models and the numerical solution in Ls-Dyna.

TEST A	
specimen width [mm]	20
bottom adherend length [mm]	65
top adherend length [mm]	25.5
overlap [mm]	20
Adherend thickness [mm]	12
Adherend material	DD11 steel
Adhesive material	epoxy

Table 2.4: *test A* joint configuration.

relevant geometry as it has been chosen for the experimental tests. Only half of the joint has been plotted being the other half symmetric. The dotted lines represent the solution of the beam theory problem, while the continuous lines are the nodal vertical displacement of the simulation. It has to be remarked that the displacement of the bottom adherend (blue line) has been translated upwards by the elongation of the adhesive layer on the outer edge. The objective of this analysis is to describe the bending deformation of the substrates that are the cause of the shear, while the adhesive displacement mostly contributes to a rigid translation of the bottom adherend. Moreover, the adhesive displacement ($\sim 1mm$) is very large if compared to the order of magnitude of the adherend displacements that are considered in this section. The other important effect of the adhesive is its compliance with the relative displacement of the two adherends that is not considered in the clamped beam model and constitutes by far the biggest assumption in this analysis. Nonetheless, the error is very small due to the fact that, while this compliance let the bottom adherend rotate more in bending, the overlap region is also made stiffer by the presence of the two adherends superposed. It can be noted that the displacements are smaller than the ones fixed in the computation of equations 2.2.3 and 2.2.7. The minimum suggested thickness

with the method above for steel ($E = 200\ MPa$), epoxy adhesive ($\sigma_a = 7.19\ MPa$) and 20 mm of overlap is: $h \simeq 7.7\ mm$. The higher thickness of 12 mm of this example correctly produced a smaller deflection that is very consistent with the analytical model shown with the dotted lines. The plot in figure 2.14 shows the results of the
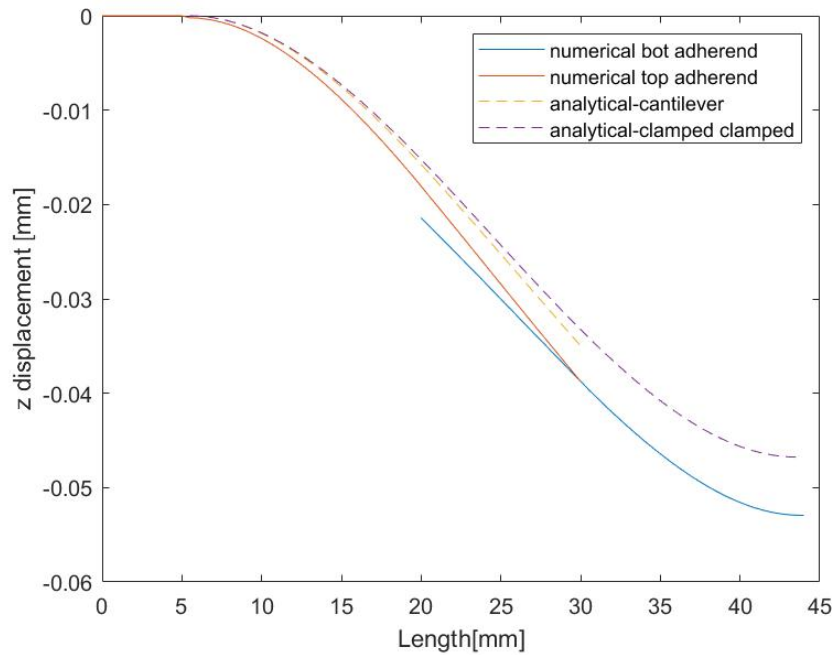

Figure 2.14: TEST with DD11 steel substrates, 7.5mm thickness, epoxy adhesive and 10mm of overlap. Comparison of the analytical solution of the two beam models and the numerical solution in Ls-Dyna.

interpolation obtained for a test with 10mm of overlap and 7.5 mm of adherend's thickness.

In conclusion, the results consistently produced very good interpolation with the numerical data, as long as the deformation is small enough. This results are particularly good for the steel substrates, thanks to the isotropic behaviour of this material. With the composite substrates the approximation of the analytical model have in
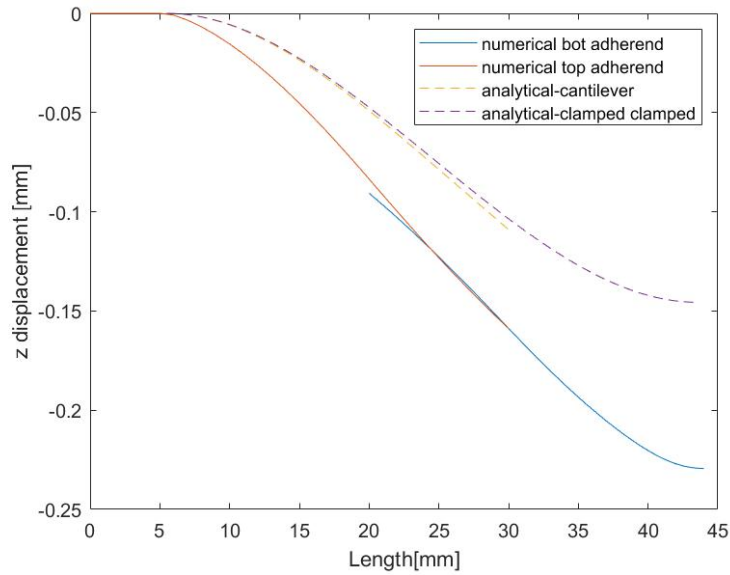
Figure 2.15: test with composite substrates (7.04mm of thickness), 10mm overlap, PU adhesive. Comparison of the analytical solution of the two beam models and the numerical solution in Ls-Dyna.

general been underestimating the deformation as can be seen in the plot in figure 2.15. This can be ascribed to the small damaging that in most cases occurred in the most stressed regions of the joint and the orthotropic behaviour of laminates. As a consequence, it is still a valuable preliminary indication for a suitable joint geometry, but it has to be taken into account that this Euler-Bernulli method is not as effective and some deeper analysis is needed. In any case, the method proved itself to be effective to easily estimate a good joint configuration for the materials under test.

Chapter 3

Results

3.1 Numerical modelling

The Ls-Dyna model was not only useful to accelerate the joint configuration opti-
mization, but also provided some interesting results that are not easily derived from
the experimental tests like the adherend bending deformation that is a key effect for
the test behaviour. Moreover, some analysis is impossible to be performed on experi-
mental data, i.e. the stress-displacement field of the cohesive elements and the crack
initiation and propagation analysis.

3.1.1 Stress-displacement analysis

A first remark on the adhesive loading condition has to prove that the designed joint
configuration in section §2.2.4 is accomplishing the requirement to have failure mode
I. A useful example for this scope is a simulation with the following joint:

- Adherend materials: DD11 steel;

- Adherend thickness: 7.5 mm;

- Adherend width: 20 mm;

- Adhesive material: epoxy;

	10mm OVERLAP	TEST A
$\sigma_p[MPa]$	7.19	7.19
$\sigma_s[MPa]$	0.186	0.155
$\delta[mm]$	0.038	0.023

Table 3.1: 10mm overlap, 7.5 mm thickness joint and *test A* comparison for the adhesive loading condition.

- overlap: 10mm.

For this overlap length and materials, the equation 2.2.3 suggests a minimum thickness of 6.2 mm. The top adherend maximum vertical displacement has been of 0.038 mm, lower the 0.05 mm specified in the geometry optimization section §2.2.4 which is aligned with the higher 7.5mm substrates thickness. The peak peel stress in the cohesive elements has been of 7.19 MPa, and the maximum shear of only 0.186 MPa. Table 3.1 reports the comparison of this test with the *test A* that has a higher thickness over-estimation.

The comparison proves that regardless materials and joint configuration, if the adherends deformation is small enough, the shear component in the adhesive can be completely neglected being the peel stress unaffected by such a small shear component and the adhesive fails by mode I.

Moreover, adhesive joints in failure mode I exhibit a fairly uniform stress distribution if compared to mixed mode and mode II, so each cohesive element had an almost superposed stress-strain field. This effect was evident in the numerical model: the tests showed that each element followed the triangular traction separation law of MAT_138 with peak stresses and displacements that resembles the failure mode I values. Also, each element deforms and fails in an almost simultaneous way as it will be further discussed in section §3.1.2. As shown in figures 3.1 and 3.2 that report the

traction separation in the numerical simulation for the epoxy and the polyurethane adhesives respectively, the peak values are the ones prescribed in the material cards (table 2.3) with 7.19 MPa of peel stress at 0.89 mm of displacement and UTD of 0.95 mm for the epoxy and 5 MPa at 1.5 mm of displacement and UTD of 1.8 mm for the polyurethane.
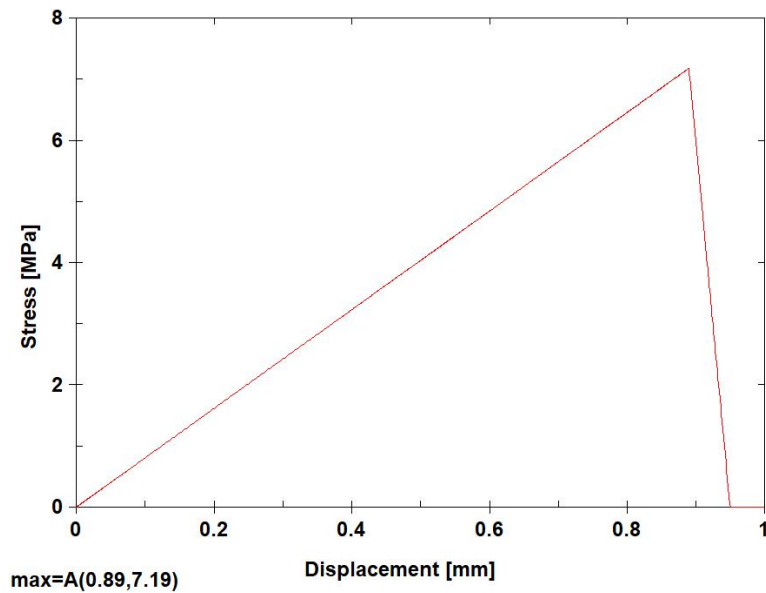
Figure 3.1: Epoxy adhesive stress-displacement in the impact test.

The traction separation law was very clean in most of the cases analysed with a continuous separation of the joined adherends from the initial contact of the dart, through the yield stress and until the end of the softening region. Some exception occurred in case the impact was at low speed and with fairly low adherends stiffness. In this cases some hysteresis is visible in the stress-displacement for some cohesive elements. This effect is caused by the induced vibration in the adherends, and particularly in the bottom one. In fact, the impact excites the touched adherend and the whole joint that starts vibrating in its first mode. From a dynamic point of view the dart provides an impulse at the centre of the specimen, in particular if considered that
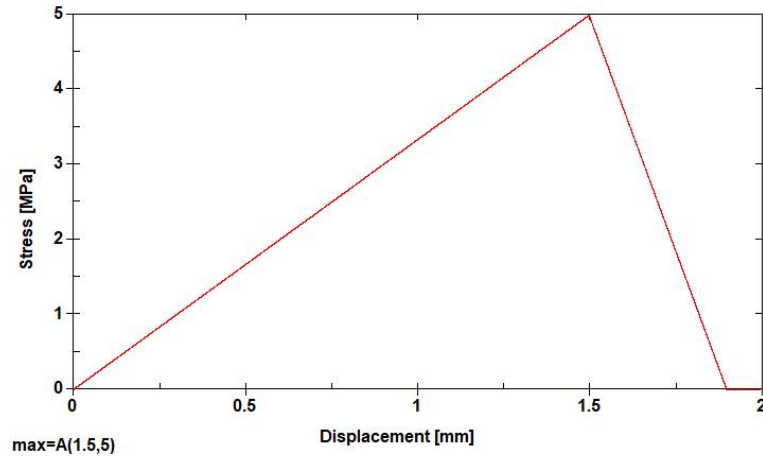
Figure 3.2: polyurethane adhesive stress-displacement in the impact test.

the whole event takes place in a very short time-frame ($0.5 \ ms \div 1.5 \ ms$) depending on the joint configuration and impact velocity. The vibration of the edges can affect the cohesive elements deformation making possible the consequent vibration of the cohesive elements. This has been noticeable only in the low velocity impacts. In fact, an increased velocity of the impactor makes the whole event faster, until a point in which it becomes faster than the natural frequency of the joint and the latter doesn't have time to oscillate before the failure occurs producing a cleaner stress-displacement curve for the adhesive. In any case, this behaviour didn't affect much the results, being the energy dissipated by adherends always the same and it never took place in the more relevant joint configurations discussed in this work. The velocity actually affects the results of the tests but this has nothing to do with vibrating phenomena and will be further discussed in section 3.1.3.

3.1.2 Crack initiation

The Ls-Dyna numerical model made possible a deep failure analysis. This analysis will be presented on the right-hand overlap and all the results will be equivalent for the

left one being the model symmetric. This assumption may lead to some errors in the experimental research for which the symmetry will be respected only at some extent and also some misalignment may occur. The numerical model exhibits a simultaneous and symmetric failure in both the bonded regions.

It is clear that for the failure mode studied the stress distribution should be quite uniform being any shear component almost absent. This is actually the case as it can be observed in the stress contour in figure 3.3 (a). The one represented is the stress close to the peak for the 10mm overlap test, steel adherends and epoxy adhesive. The percentage delta in stress between the most and the least loaded element is limited to about 1%. There is still a minor stress concentration towards the outer edge and corners that will eventually lead to the crack initiation.

Focusing on the stress contour right before failure in figure 3.3 (b), it can be seen that the most loaded region at peak stress is now the least loaded one, having now reached the end of the softening region. At this moment, the stress gradient is significantly higher but it only depends on the adhesive material: the epoxy adhesive of this model has a very steep softening region, and being all the separation displacement driven, the same delta displacement between the inner and the outer edge of the peak stress, here produces a much higher delta of the stress. Right afterwards, the failure starts and quickly propagates following the stress contour. All the failure is very fast also if compared with the already quick impact duration, the deletion of all the cohesive elements takes place in about 10^{-6} s.

The analysis on the 20mm overlap *test A* in the figures 3.4, 3.4 reveals that the failure starts at the inner edge of the bonding. The behaviour is exactly the same but symmetric, in this case with a stress concentration on the inner edge and slightly towards the corners. As already remarked the failure is displacement driven and the

(a) *8 mm overlap*   (b) *4 mm overlap*
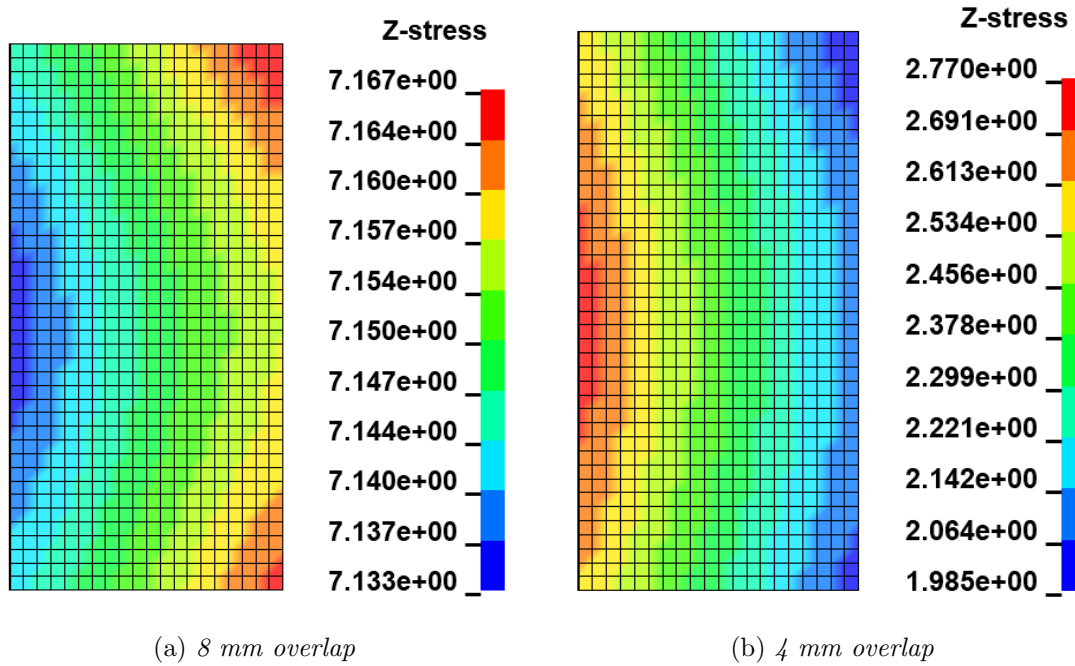
Figure 3.3: *10mm overlap, DD11 steel substrates and epoxy adhesive:* Peel stress contour at peak adhesive stress (a) and before failure (b).

region that will reach before the UTD will nucleate the crack. Whether this is the inner or the outer edge has to do with the geometry, and in particular, with the relative rotation of the bonded adherends. This difference can be highlighted comparing the figure 2.13 with figure 2.14 in section 2.2.4. The distance between the two numerical solution in the overlap region in this plot represent the delta displacement of the adhesive. It can be seen that the 10mm overlap test in fig. 2.14 the top adherend is slightly more bent and consequently the crack initiates on the outer edge. This is the behaviour of the optimized geometry, for which the centre of the overlap is at 20 mm from the support, balancing the bending stiffness of the adherends; which is slightly higher for the bottom one to leave some room to bear the concentrated load of the dart. On the contrary, in the 20mm overlap test it's the bottom adherend to bend more initiating the crack on the inner edge. The discrepancy is due to the

test A geometry, that to allow a 20mm overlap and leaving sufficient space for the dart to impact the lower adherend, has moved the center of the overlap towards the support (at 15.5 mm) making the bottom adherend longer than its optimal length and consequently its bending stiffness is lower than the one of the top adherend.
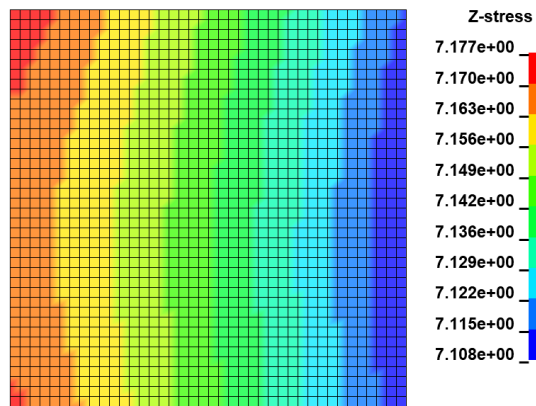
Figure 3.4: *Test A*: Peel stress contour at peach adhesive stress.
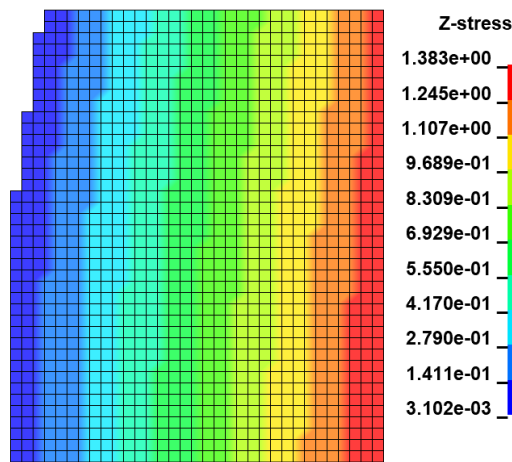
Figure 3.5: *Test A*: Peel stress contour at failure initiation.

3.1.3 Energy analysis

The energy absorbed under failure by the specimen is the most important data in an impact test. This is the main piece of information obtainable by experimental tests without auxiliary equipment. The numerical simulation also in this case was able to analyse more deeply the behaviour of the joint thanks to the solved stress-strain field during the computation. In this work it was used to find out what part of the dissipated energy is being absorbed by the failing adhesive or by the deformable substrates and which parameters are affecting the results. It has to be remarked that being the one studied a test on a complete joint, the results depends on adhesive and adherends properties both.

In the experimental tests this value is obtained by subsequent numerical integration of the force data recorded by the load cell and will be further discussed in section 3.2. The total energy absorbed in the numerical simulation resulted to be equal to the dissipated kinetic energy of the dart. The typical trend of the dart kinetic energy in shown in figure 3.6. At the beginning of the simulation the kinetic energy is constant and it is function of the selected impacting parameters ($E_k = \frac{1}{2}m \cdot v^2$). Once the contact is established the dart velocity is slowly worn-out as function of the contact force. This trend can be not very progressive because the contact with a rigid body (dart) in Ls-Dyna is quite harsh and can cause high peaks of force followed by the momentary lose of contact. At 0.8 ms the failure occurs, the bottom adherend is detached not exploiting any more resistance to the impactor that keeps its residual velocity and energy until the end of the simulation. The difference between this ending constant energy and the initial one is the dissipated energy that in the example in figure 3.6 is $E_a = 3.42 \ J$.

The first part of the present analysis aims to investigate the energy absorption
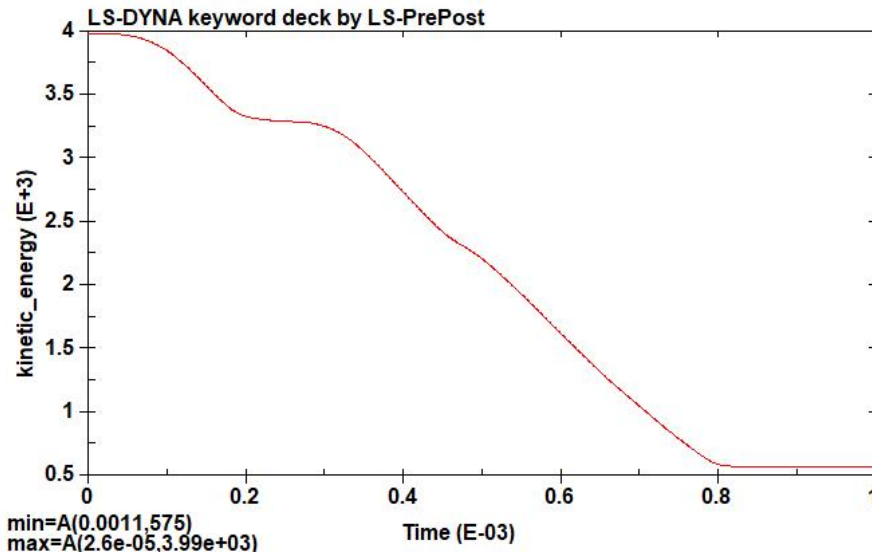
Figure 3.6: Dart kinetic energy during the impact evolution for *test A*.

through the impact duration by the main entities, namely, adhesive and adherends. Beyond these two components there is only friction and hourglass energy. The latter is a computational necessary energy for solid elements formulation 1. Its value is kept as low as possible and didn't exceed 80 mJ and can be considered negligible. Friction coefficient have been fixed to 0.2 on every sliding interface (dart to adherend and adherend to rigidwall) but being the sliding fairly limited and the test duration very quick also this component is negligible ($E_{sl} = 5\ mJ \div 10\ mJ$).

In figure 3.7 is shown the trend along the test of *the total energy* for adhesive and adherends in the same test A with 4J of provided energy. The most important region of this plot is after the failure of the specimen occurs, when the energy of each component reaches its constant final value. These values are reported in the table 3.2 also compared with the absorbed energy of the same test.

The first important result is that the energy absorbed by the adhesive account for the most part of the dissipated energy. Moreover, this quantity is all internal energy, i.e. *strain energy*. It's value of 2.73 J is exactly the expected one known the
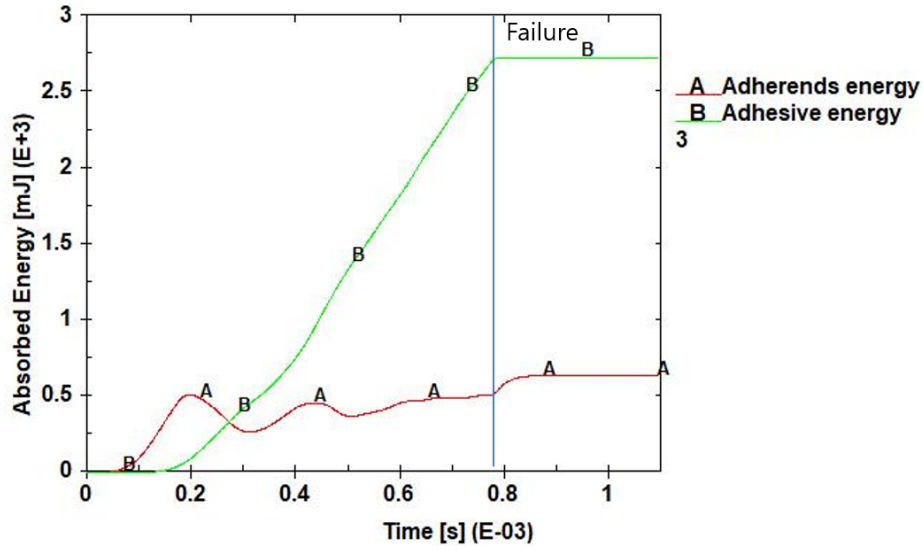
Figure 3.7: *Test A* (20mm overlap) energy absorption of adhesive and adherends in the impact duration.

	energy $[J]$	$E_i/E_a\%$
$E_{absorbed}$	3.42	
$E_{adhesive}$	2.73	80%
$E_{adherend}$	0.63	18.5%
E_{sl+hg}	0.05	1.5%

Table 3.2: *test A* joint configuration.

failure mode I energy release rate of the epoxy adhesive: GIC times the surface area of adhesive for both the bonding regions.

$$E_{adhesive} = 2 \cdot GIC \cdot ovl \cdot b \qquad (3.1.1)$$

An other positive result is that the adhesive absorbs 80% of the total absorbed energy, leaving to the adherends a contribution that is lower than 20%, which is definitely good for a test on complete joints that aims to identify the adhesive material properties. In reality this ratio may change with joint configuration and impacting energy and will be further discussed in the section 3.1.4.

The adherends contribution is not as simple to describe. It doesn't dissipate energy only by strain, but also by accumulating kinetic energy. Moreover, the bottom adherend dissipates 0.62 J of energy which accounts for more than 98% of the total adherends absorbed energy ($E_{adherends}$ in table 3.2). In fact, the two top adherends can only absorb a small amount of energy by elastic strain until the adhesive fails and they start free vibrations but at this moment they don't affect the test any more. This adherends doesn't exhibit any plastic strain as it was designed in the specimen geometry optimization. On the other hand, the bottom adherend bears the concentrated load of the impactor and most of the energy is dissipated in the creating indent by plastic deformation. Figure 3.8 shows the strain along the length of the adherend on the top surface. The strain is close to 10% where the dart hits. The consequent plastic strain is capable of dissipating a lot more energy in this limited area than the elastic deformation by bending of the rest of the adherend.

Figure 3.9 shows how small the contribution of the fixed adherend is to the absorbed energy. Only a small amount of elastic strain energy is accumulated and suddenly released as soon as the adhesive fails ($t = 0.79 \ ms$). At this moment the
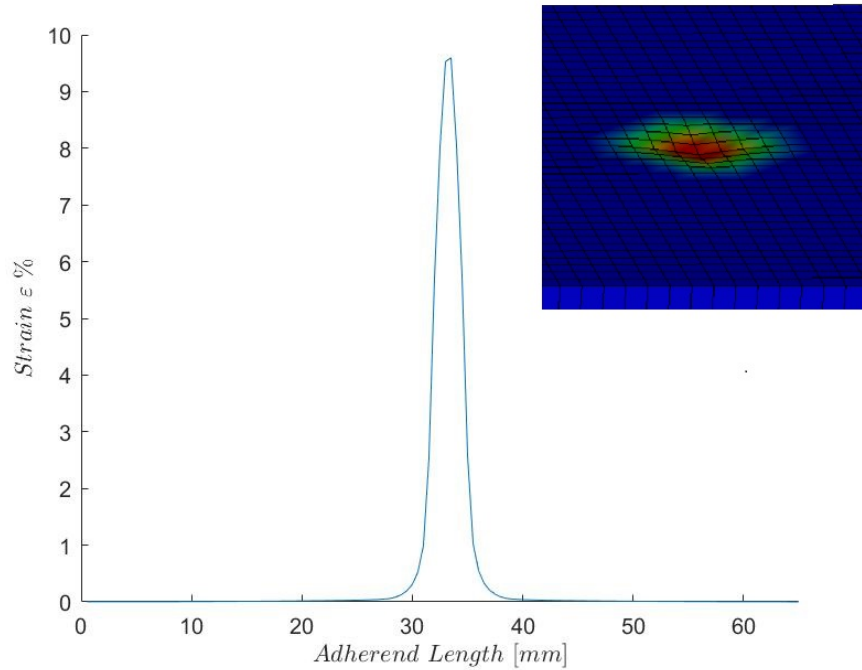
Figure 3.8: *test A* strain along the upper mid surface, the strain is close to 10 % in the indent region.

top adherends starts free oscillation shown in the energy graph by the continuous conversion of strain energy into kinetic energy. More complex and more relevant are the curves for the bottom adherend (B and D) that can be studied in three regions:

- $t = 0 \ ms \div 0.3 \ ms$: in this phase the contact with the dart is initiated, there is a sudden spike in kinetic energy being the part accelerated by the elevated initial contact force and slowed down only by the adhesive reaction that initially is quite compliant.

- $t = 0.3 \ ms \div 0.79 \ ms$: in this phase the adhesive is being stretched and can oppose an increasing force that bends the adherend accumulating strain energy. As a consequence also the dart exhibits an increasing force and most of the energy is dissipated in this phase.

- $t = 0.8\ ms \div end$: the almost sudden failure of the adhesive leaves the adherend without any constraint, it releases some of the elastic strain energy and is quickly accelerated like a spring being still in contact with the dart.
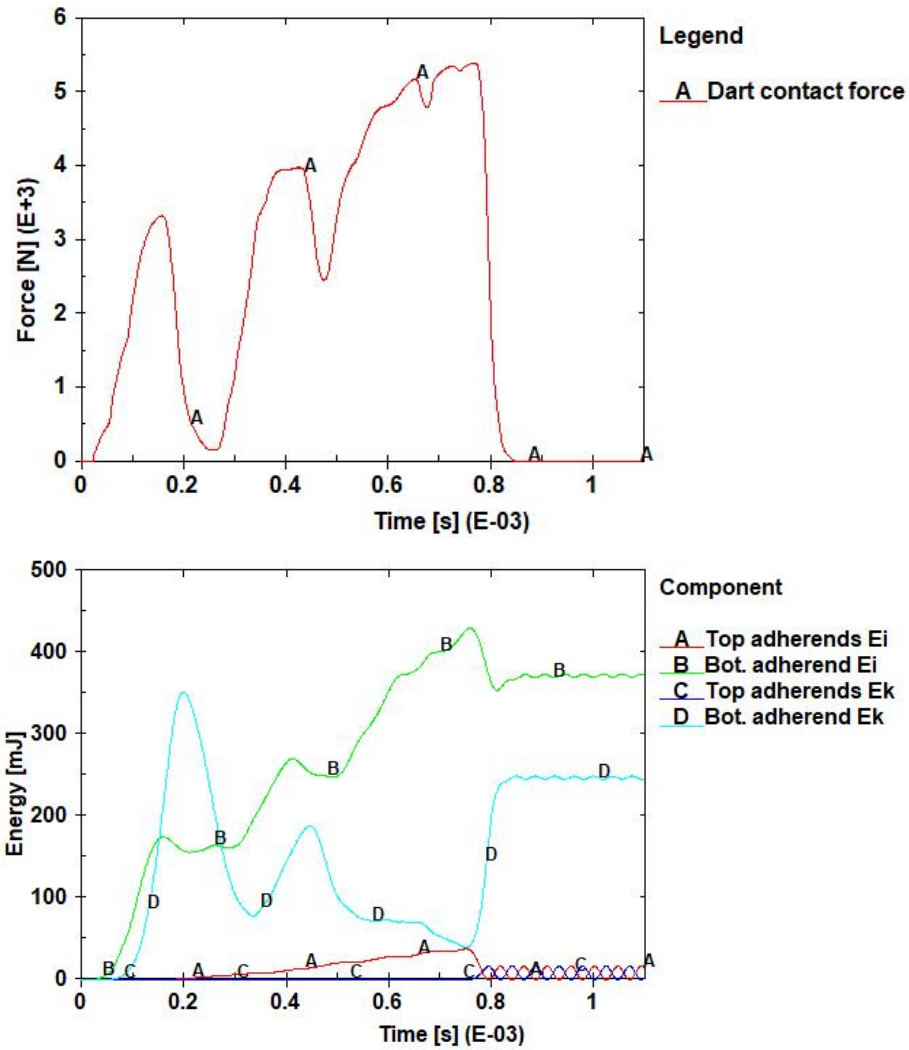
Figure 3.9: Kinetic and internal energy in the test duration for the fixed and the bottom adherend.

3.1.4 Effect of dart velocity

In this section the effect of different impactor energy and velocity is discussed. The analysis have been performed on the same test configuration A with epoxy adhesive discussed before. The adhesive and adherends both does not have any strain rate dependent material properties. Nonetheless, some remarkable results have been highlighted; Some repeated tests have been performed keeping a fixed impactor mass of 2 *kg* and progressively increasing the velocity from a quasi-static test up to 4 *m/s* or rather an impacting energy of 16 *J*. The quasi-static tests have been performed with the same specimen configuration by assigning a *prescribed motion* to the dart instead of an initial velocity. This constant velocity of the impactor has been set to 1 *mm/min*. The data are summed up in table 3.3. It can be observed that regardless the materials which are not strain-rate dependent, the changing velocity of the dart changes, in turn, the joint's absorbed energy as can be clearly seen in the plot in figure 3.10. This behaviour is all accountable to dynamic effects: the higher the impactor velocity is, the harsher the impact results to be. An increasing velocity makes the test duration quicker and the forces involved higher, inducing a bigger deformation in the adherends and a more severe indent that progressively increases the strain energy of the adherends. This strain energy effect is for the most part, function of the impacting energy.

On the other hand, the energy absorbed by the adhesive is constant regardless the test velocity, direct consequence of the failure of each cohesive element that dissipates exactly the material energy release rate defined in the material card. The quasi-static test acts as a lower bound of the absorbed energy, showing that a minimum of about 10% of the absorbed energy is going to be dissipated by the substrates, regarding this particular materials, and joint configuration; but the adherend contribution appear

Test A				
Provided energy [J]	16	8	4	quasi-static
Absorbed energy [J]	5.24	4.08	3.42	3.20
Ei adhesive [J]	2.73			
Ei Adherends [J]	0.98 (19%)	0.50 (12%)	0.38(11%)	0.28 (9%)
Ek adherends [J]	1.43(27%)	0.79 (19%)	0.25(7%)	0
E total Adherends [J]	2.41 (46%)	1.29 (32%)	0.63 (18%)	0.28 (9%)

Table 3.3: *test A* effect on impactor energy.

to increase up to a 40% contribution exhibited in the highest velocity test performed.
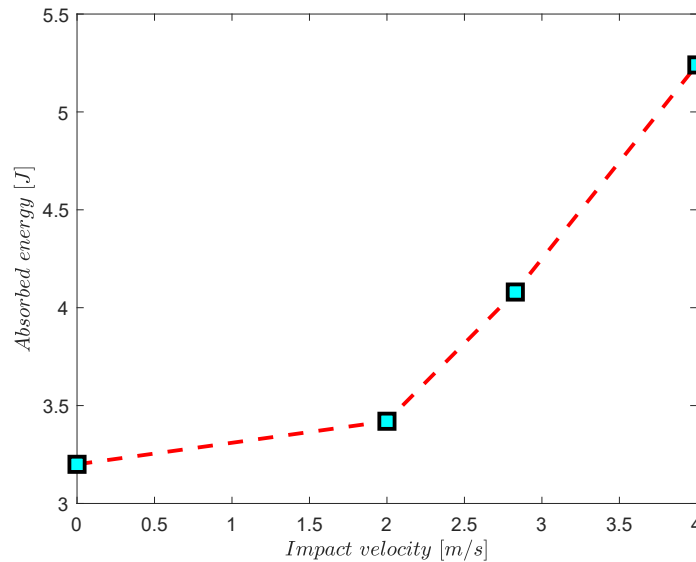
Figure 3.10: Test A: Effect of dart velocity on absorbed energy. The value at null velocity is the quasi-static test.

This test is presented with the commonly adopted procedure in impact tests with drop dart testing machines: using a fixed impacting mass and progressively increasing the impactor velocity. But to highlight the role of the dart velocity rather than the provided energy some simulations have been run with fixed 4J energy level but with scaled velocity and mass for the same *test A* configuration. The results in table 3.4

	$M = 16.3\ kg$ $v = 0.7\ m/s$	$M = 2\ kg$ $v = 2\ m/s$	$M = 1\ kg$ $v = 2.82\ m/s$	$M = 0.5\ kg$ $v = 4\ m/s$
Provided energy [J]	4	4	4	4
Absorbed energy [J]	3.29	3.42	3.57	3.82
Ei adhesive [J]			2.73	
Ei Adherends [J]	0.27 (8.2%)	0.38 (11.1%)	0.50 (14.0%)	0.82 (21.5%)
Ek adherends [J]	0.25 (7.5%)	0.25 (7.3%)	0.26 (7.2%)	0.19 (5.0%)
E tot. Adherends [J]	0.52 (15.8%)	0.63 (18.4%)	0.76 (21.2%)	1.01 (26.4%)

Table 3.4: *test A* effect on impactor velocity.

and the trend in the plot in figure 3.11 show a very similar behaviour to the one described before regardless of the constant energy provided with a trend that in this case is close to be linear.

The behaviour becomes more complex whether the MAT_240 with strain-rate is used. In this case the energy dissipation of the adhesive would decrease with the increasing test velocity, while its strength would increase, rising, in turn, the substrates stress and deformation. This means that there are two behaviours that go in opposite directions, making them difficult to be isolated.

3.1.5 Effect of joint configuration

Most of the analysis performed up to this point is referred to the *test A* joint configuration. The main effects discussed are recognisable in other configurations and materials but their magnitude changes consequently. In this section the results by using the polyurethane adhesive, the joint with 10mm of overlap and composite material substrates are further discussed.

In the table 3.5 are reported the energy data at different impactor energy levels for the test with 10mm of overlap, now called *test B*, that has the following geometry
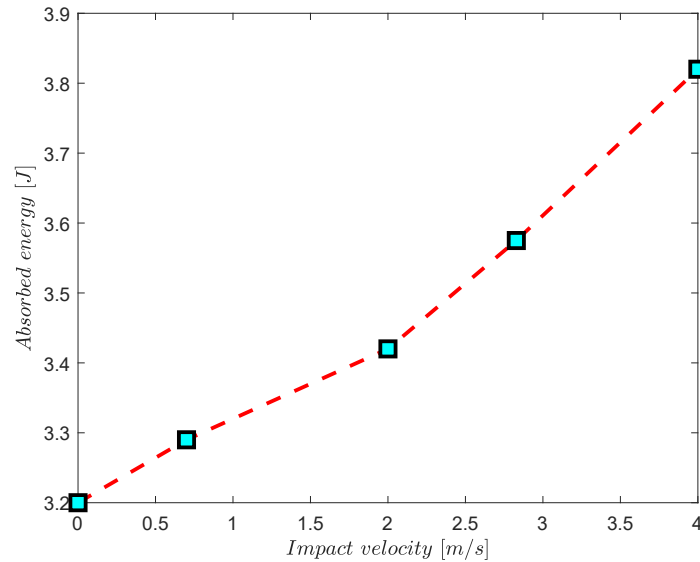
Figure 3.11: *Test A*: effect of dart velocity with constant provided energy of 4J.

characteristics:

- Adherends thickness: 7.5mm;

- Adherends width: 20 mm;

- Adherends material: DD11 steel;

- Overlap: 10mm;

- Adhesive material: epoxy.

The same method used for test A has been adopted in this case: The impactor mass was fixed at 2 kg, and the velocity has been progressively increased starting from a quasi-static test at 1mm/min. As it can be observed in the comparison in figure 3.12, this configuration follows the same behaviour analysed before, with the absorbed energy that increases with the increased impactor energy and velocity. On the other

	test B			
Provided energy [J]	8	4	2	quasi-static
Absorbed energy [J]	1.99	1.85	1.69	1.49
Ei adhesive [J]		1.37		
Ei Adherends [J]	0.265 (13%)	0.197 (10%)	0.124(7%)	0.114 (8%)
Ek adherends [J]	0.330(17%)	0.270 (15%)	0.182(11%)	0
E total Adherends [J]	0.595 (30%)	0.467 (25%)	0.306 (18%)	0.114 (8%)

Table 3.5: *10mm overlap test*: effect on impactor energy.

hand, the magnitude of this phenomenon is quite different, starting from the quasi-static test, the adherend contribution is limited to the 8% of the absorbed energy, and it doesn't increase as steeply as in the 20mm overlap configuration. This is a direct consequence of the lower forces involved with the reduced overlap that is not able to impress any significant plastic deformation in the substrates. Moreover, it has to be considered that the test B configuration is less stiff if compared to the test A joint. Comparing figures 2.13 and 2.14, the test B substrates has about double the vertical vertical displacement of the adherends than test A (test A: 0.025 mm, test B: 0.05 mm). The more compliant adherends reduce the peak force of impactor and further increase the effect on the absorbed energy discussed.

An other interesting comparison is shown in table 3.6 in which the same test B specimen bonded with the epoxy adhesive is compared in an equivalent test but joined with the polyurethane one. As show in the material cards 2.3, this material has a lower strength, but a significantly larger UTD and ultimately a larger energy release rate. The direct consequence of the mechanical properties is that the energy absorbed by the joint is increased due to the higher contribution to the energy dissipation of the adhesive failure; The internal energy of the adhesive is still equal to the energy
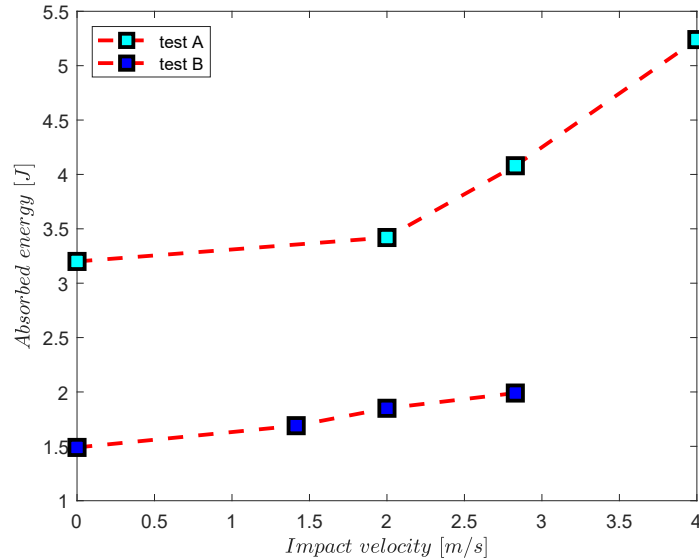
Figure 3.12: Comparison between the absorbed energy as function of the impactor velocity for *test A* and *test B*.

release rate times the overlap area (cf. equation 3.1.1) that for the PU adhesive is 1.9 J against 1.37 J of the epoxy. On the contrary, the adherend contribution is reduced: due to the lower strength of the adhesive and its higher compliance, the forces are reduced and the substrates are deformed less. Taking as reference the maximum vertical displacement of the clamped adherends it resulted to be 0.025 mm for the PU test and 0.04 mm for the epoxy one.

An investigation on composite material substrates is here discussed. The material is the carbon fibre whose mechanical properties are shown in the table 2.2. The considered laminate was made by 8 layers of fabric for a total thickness of 7.04mm and the specimen characteristics are highlighted in table 3.7.

The joint stiffness is significantly lower than the one investigated before: as can be seen in figure 2.15 for example the clamped adherends bends by about 0.1mm while

	test B Epoxy	test B PU
Provided energy [J]	4	4
Absorbed energy [J]	1.85	2.20
Ei adhesive [J]	1.37	1.90
Ei Adherends [J]	0.197 (10%)	0.144(6.5%)
Ek adherends [J]	0.270 (15%)	0.130(6%)
E total Adherends [J]	0.467 (25%)	0.274 (12%)

Table 3.6: *10mm overlap test B configuration*: Details on absorbed energy with the epoxy and the polyurethane adhesive.

TEST C	
specimen width [*mm*]	20
bottom adherend length [*mm*]	48
top adherend length [*mm*]	24
overlap [*mm*]	10
Adherend thickness [*mm*]	7.04
Adherend material	CFRP
Number of layers	8
Adhesive material	PU

Table 3.7: *test C* joint configuration.

the test A and test B bends of 0.01 and 0.03 mm respectively. This is due to the underestimated substrates thickness (the analytical method suggests a thickness of 8.4 mm). This higher bending deformation is known to increase the shear component in the adhesive layer but, as show in figure 3.13, this component is still limited to 0.26 MPa (2.6% of the ultimate shear strength) that still produces a negligible mixed mode component and failure for traction that resembles the mode I traction separation law.
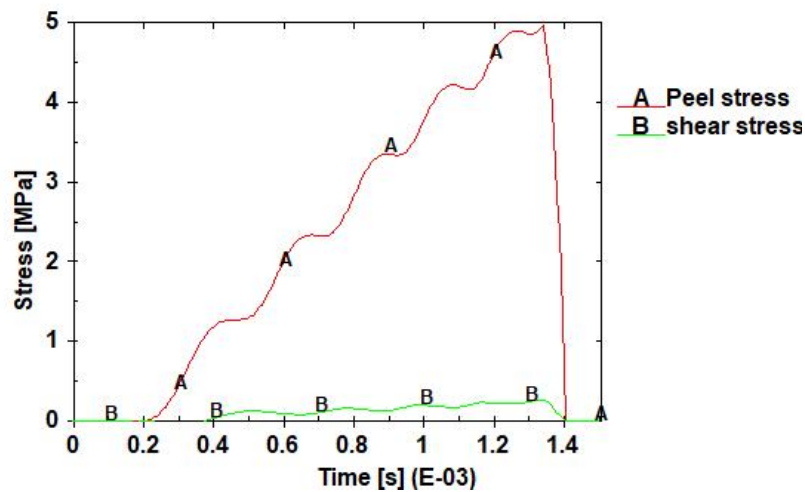
Figure 3.13: Peel and shear stress components of the adhesive in the 10mm overlap test with composite substrates.

This configuration is quite on the edge of admissibility, in fact it's enough to use the epoxy adhesive that is stiffer and slightly stronger to make the failure condition unacceptable. The peak shear stress even exceeds the peak peel and the adhesive fails in mixed mode. In fact, the bending deformation would be significantly higher with the clamped adherends displacement that reaches 0.6 *mm* and severe damaging is reported in the composite substrates.

The energy data with the same methodology applied in test A and B (2kg of impacting mass and progressively incresed dart velocity) is reported in table 3.8. As expected the same behaviour exploited with the other materials is still present, with an

increased adherends contribution to the absorbed energy with an increased impactor velocity, but some phenomena can be observed on the behaviour the substrates. As shown in figure 3.14, a significant peak in strain energy is reached for the clamped and the bottom adherends both because, on the contrary of test A (cfr. figure 3.9), in this configuration the bending stiffness is well balanced between the three adherends. This is mostly elastic energy that is accumulated under the load, released and converted in kinetic energy once the adhesive fails at $t = 0.9 \ ms$. At this moment the clamped adherends strain energy starts oscillating being now subjected to its free vibrations and its energy that touches the zero is the consequence of the negligible material damaging reported.
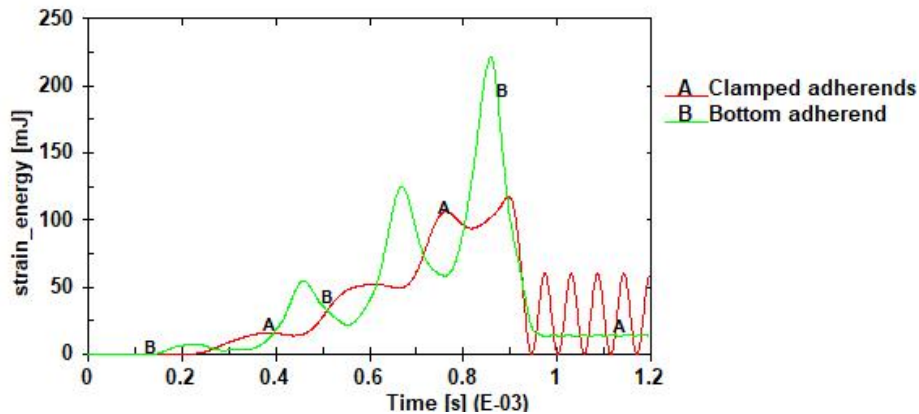
Figure 3.14: Test C: strain energy evolution for the clamped adherends (top) and the bottom one.

The bottom adherend, once the adhesive fails, also releases most of the accumulated strain energy and the small residual amount of it at the end of the simulation is due to the small material damage in the impacting region (a maximum of 0.2%). As shown in figure 3.15, at the joint failure the detatched adherend quickly gains kinetic energy in the same way but even at a greater extent than reported for test A (cfr. figure 3.9). This is due to the elastic properties of this kind of composite

	test C		
Provided energy [J]	8	4	2.5
Absorbed energy [J]	2.35	2.29	2.12
Ei adhesive [J]		1.90	
Ei Adherends [J]	0.051 (2%)	0.065 (3%)	0.040(2%)
Ek adherends [J]	0.389(17%)	0.316 (14%)	0.176(8%)
E total Adherends [J]	0.440 (19%)	0.381 (17%)	0.216 (10%)

Table 3.8: *test C: 10mm overlap, PU adhesive, composite substrates.* Effect of impactor energy.

material (lower elastic modulus) and the overall smaller bending stiffness of this joint. In conclusion, it has to be remarked that even if the values of internal energy at the end of the event reported in table 3.8 are very small it doesn't mean that the elastic deformation of the substrates is small too.
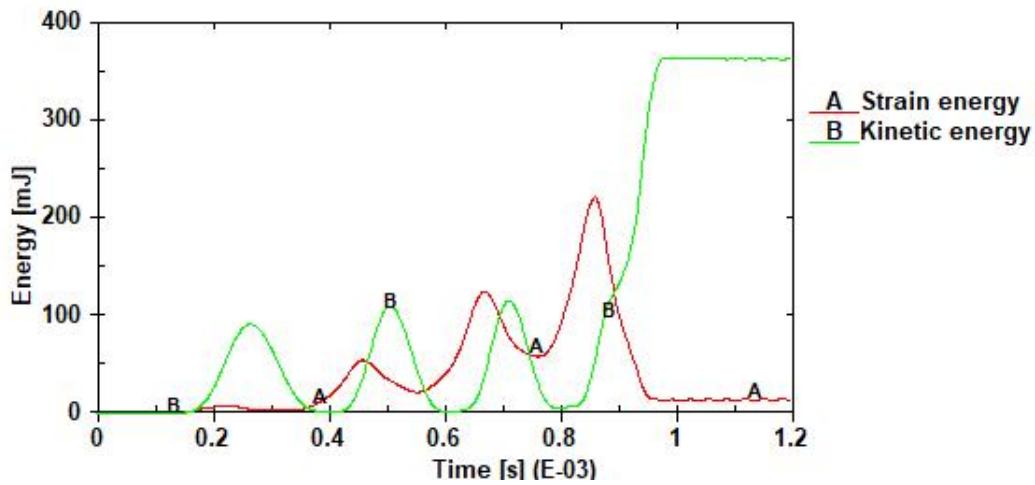
Figure 3.15: Test C: bottom adherend strain and kinetic energy evolution.

This configuration can also be compared with the the *test B*: they have in common the overlap length and the geometry, even the thickness is similar, but both the adhesive and adherends material are different. As shown in figure 3.16 the composite joint can dissipate more energy but this is completely assignable to the greater energy

dissipated by the PU adhesive compared to the epoxy one. On the other hand the higher strength of the CFRP that almost doesn't report any damaging contributes less to the absorbed energy than the mild steel counterpart that is easily plastically deformed under the impactor force.

(a) *Absorbed energy*
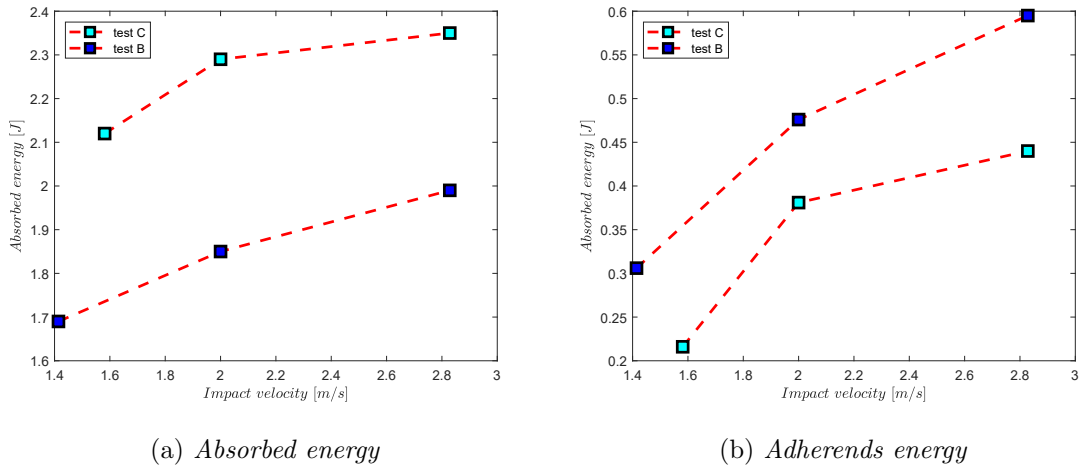
(b) *Adherends energy*

Figure 3.16: Total absorbed energy and energy absorbed by the substrates comparison between test B and test C.

This result is the effect of the sum of contributions that go in opposite way:

- A higher adhesive strength increases the adherends absorbed energy;

- A higher strength substrate reduces the adherends absorbed energy;

- More compliant substrates increase their absorbed energy;

- Plastic deformation, even if localized, strongly affects the energy dissipated.

For example, as show in figure 3.17, the same test B bonded with the PU adhesive, the substrates only contribute for 12% of the dissipated energy instead of the 17% of test C whose composite substrates are significantly more compliant. To conclude, the test discussed in this work is not only affected by the mechanical properties of the

tested materials on their own, but even on their combination and their ratio, in terms of strength and stiffness of adhesive and substrates.
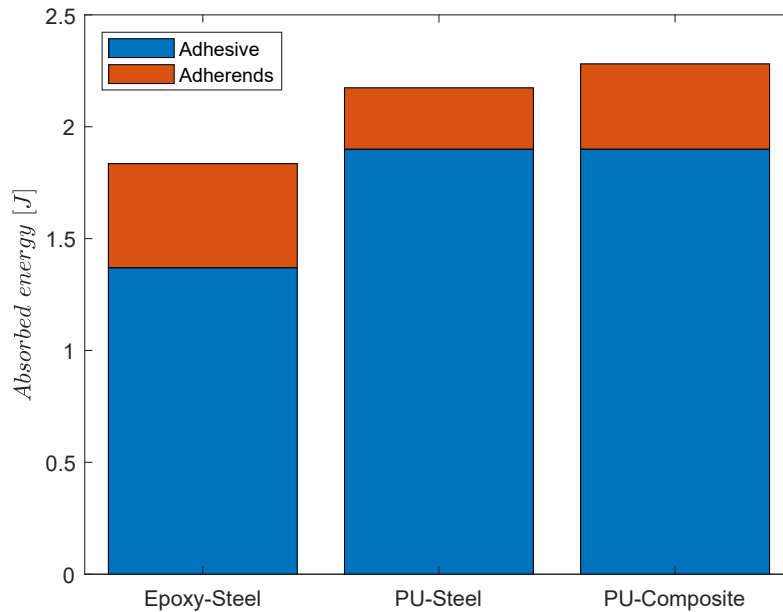
Figure 3.17: Energy absorbed by the adhesive and adherends in the 10mm tests with epoxy adhesive-steel substrates, PU adhesive-steel substrates, PU adhesive-composite substrates. Tests with 4J of provided energy.

3.1.6 Impacting force

The force registered by the load cell is not only the data from which the absorbed energy is computed in the experimental tests, it is also a valuable data on its own. In this section the results obtained from the numerical model regarding this parameter are discussed.

While in the quasi static tests the trend of the applied force resembles the adhesive traction separation law, under dynamic loading condition this can change a lot. In figure 3.18 it is plotted the trend of the force during the impact tests for simulations

at different velocities of test A. It can be observed that all the data are subjected to large oscillations with two large peaks before $t = 0.4\ ms$. Due to the fact that, regardless the impactor velocity, this two spikes are almost superposed in time, it is clear that the phenomena has to deal with the natural frequency of the system. The substrates are much stiffer than the adhesive being them subjected to a maximum bending displacement of 0.03 mm (c.f. 2.13) while the epoxy adhesive UTD is much larger at 0.95 mm; As a consequence when the impact occurs the bottom adherend is quickly accelerated, almost losing contact with the dart, until the adhesive can react with a sufficient opposing force and a strong contact is re-established. In case of 4 m/s test, in which the event correctly takes place in about half of the 2 m/s test duration, it's almost like two twin impacts occurs. But this phenomena is only a consequence of this particular combination of velocities and joint inertia.
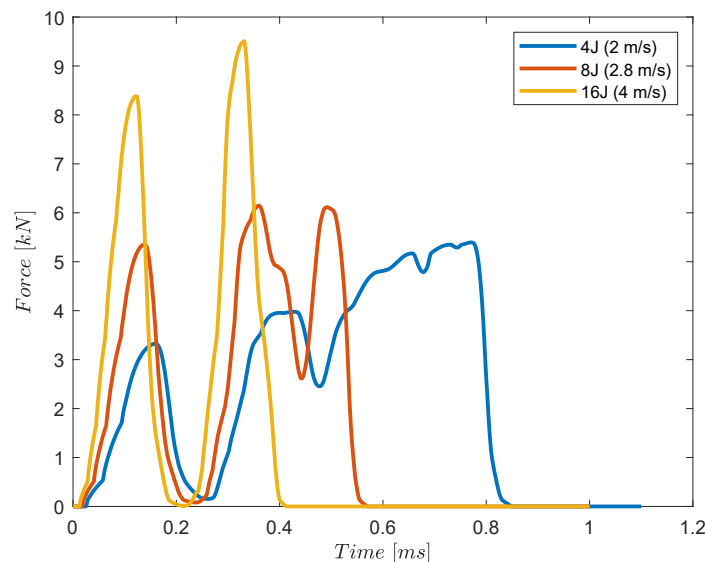
Figure 3.18: *Test A, constant mass*: Impact force-time plots for the test at 4J (2m/s), 8J (2.8284 m/s), 16J (4m/s).

Analysing the peak force value, for the configuration of *test B* it has been recorded

a minimum value of the impact force in the quasi static test, that progressively increases with the dart velocity according to the impulse behaviour of the force in a dynamic test. The force is the quasi static test has been 2.98 kN; a reasonable value that can be compared with the maximum theoretical force exploited by the adhesive that is the peel strength times the bonded surface area:

$$F_{max} = 2\sigma_p \cdot b \cdot Ovl = 2.876 \ kN \tag{3.1.2}$$
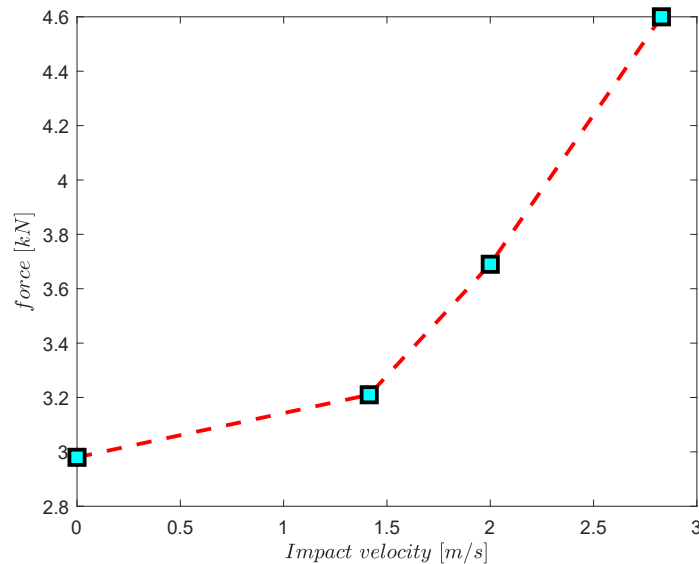
Figure 3.19: Impact test on specimen B with 2kg impactor mass and progressively increased velocity, dart contact peak force versus dart velocity.

An unexpected behaviour has been recorded on test A. As shown in figure 3.20 in the quasi static test the 5.76 kN are perfectly aligned with the theoretical epoxy adhesive strength that for 20 mm of overlap is 5.752 kN. Moving to the dynamic tests, a decrease in the peak force has been noted in the lower velocity range, to exploit a steep increase of the value between 2 and 4 m/s. Also the plot of the tests performed at constant mass, with a progressive increase of the impactor energy, and

the one of the simulations at constant provided energy (4J) are almost superposed, revealing how the impact force is strictly correlated with the impactor speed, rather than its kinetic energy.
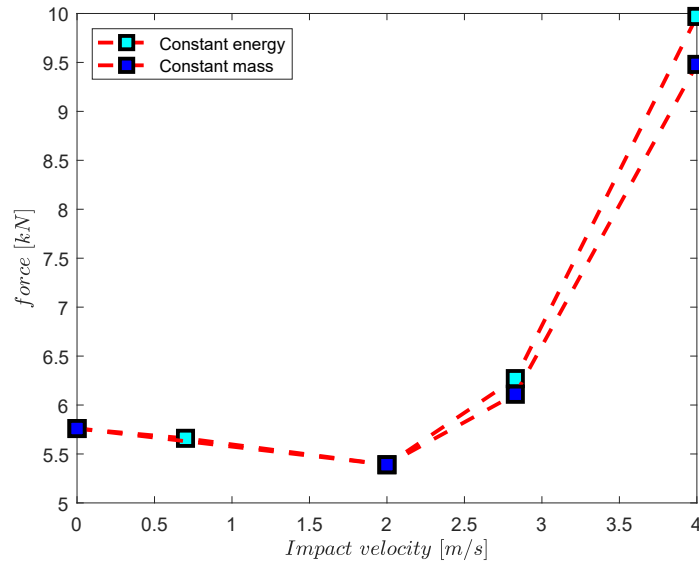
Figure 3.20: Impact test on specimen A with 2kg impactor mass and progressively increased velocity (constant mass), and constant 4J of provided energy with scaled mass (constant energy). dart contact peak force versus dart velocity.

The atypical force decrease at 2m/s is referable to the accumulated momentum of the bottom adherend at the peak force time. In figure 3.21 it is plotted the impacting force together with the equivalent rigid body velocity of the detaching adherend. It can be observed that as soon as there is a spike in the force the adherend is accelerated; whether the contact with the dart is not as strong, it is slowed down by the opposing force of the adhesive. Focusing on the moment close to failure (t = 0.78 ms) the adherend has a non negligible velocity of about 1 m/s and contributes with its momentum to the failure of the joint and ultimately reducing the impact peak force. This effect is still present in the higher velocity tests but it is completely overcome

by the much stronger impulse of the force.
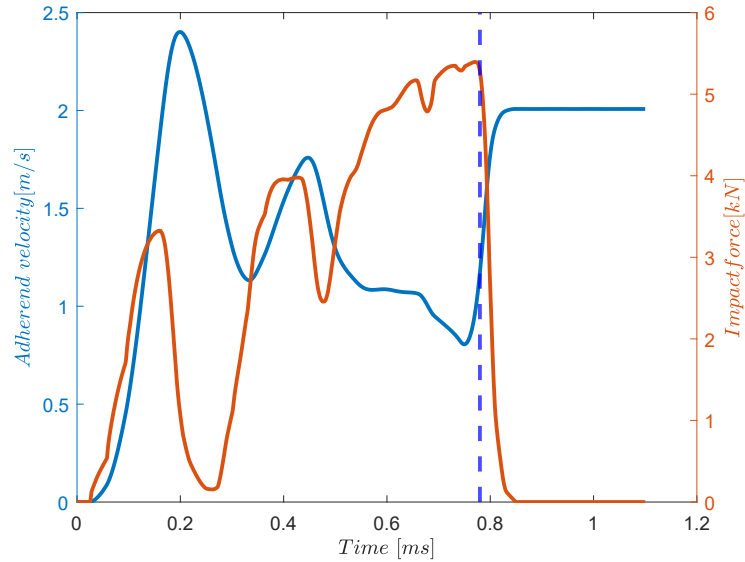
Figure 3.21: Impact: 4J (2m/s), test A: bottom adherend equivalent rigid body velocity and impating force. The Adherend velocity at failure (t = 0.78 ms) contributes to keep the force low thanks to its momentum.

The impacting force is known to be proportional to the specimen strength and stiffness. The comparison of the impact force for test B and C in figure 3.22 was predictable according to this assumption; the joint C is more compliant regarding the substrate material and the PU adhesive both. As a consequence, regardless the higher energy dissipated by this configuration, the maximum force registered is significantly lower than test B.
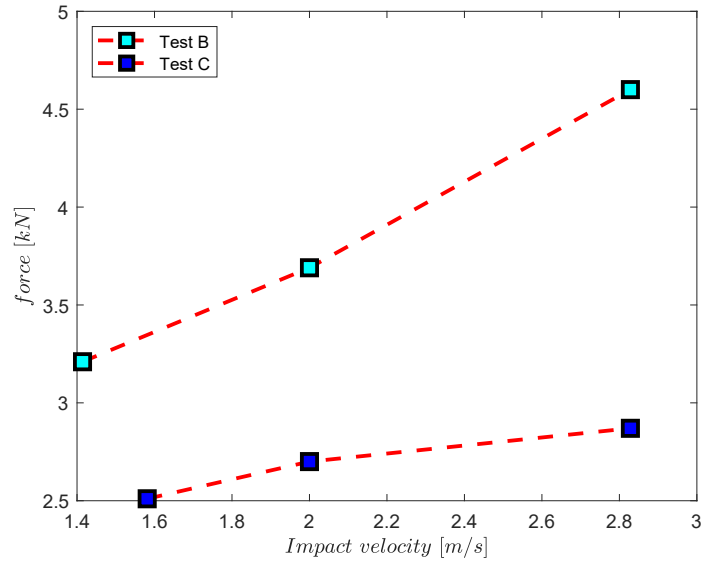
Figure 3.22: Comparison of impact force-impactor velocity for test B and test C.
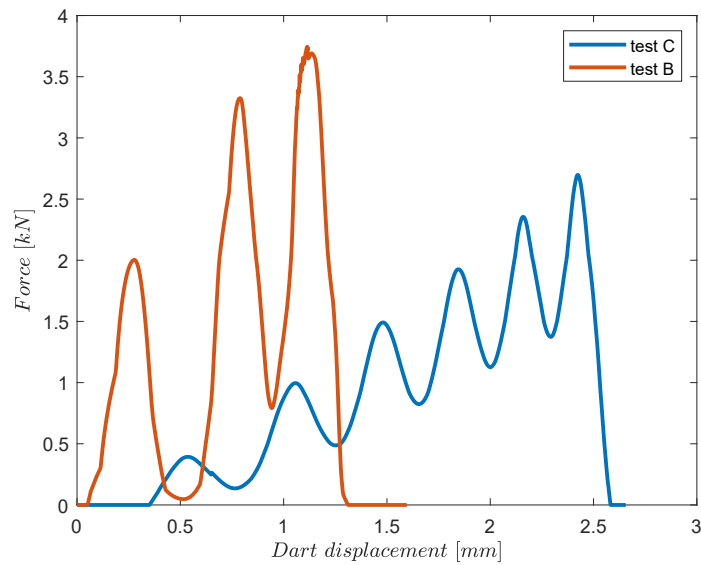
Figure 3.23: *Test B and test C at 4J impacting energy:* dart force-displacement.

3.1.7 Strain rate effect

Many engineering materials are known to exhibit significant change in material properties under large strain rate. In particular they behave in a more brittle way, with an increase in modulus and a reduction of elongation. As a result the energy absorbed during the impact is usually reduced. This numerical model is ready to implement this effect by swapping to material model that account for strain rate. Both adhesive and substrate affect the result of this kind of test but in any case the test have been designed so that the main role is held by the adhesive that contributes up to the 90% of the energy absorbed in the impact test. As a consequence the possible implementation of mat_240 is discussed in this section.

This material model is known to be one of the most established that can account for strain rate in cohesive elements, in the dedicated section §1.5.2 are reported its main characteristics. Due to the trilinear traction separation law with plasticity even the static properties of mat_138 has to be modified. A first interpolation of the cited Arcan test is shown in figure 3.24. The energy release rate and the ultimate displacements in mode I and mode II have been kept equal to the experimental test data and to the mat_138 model, as a consequence the trilinear model has a slightly reduced strength.

In this work it was not possible to further develop the model because a deeper material characterization is needed in order to estimate the strain rate properties of the materials under test; the implementation of Mat_240 in the numerical model is the main future development to accomplish.

(a) *Mode I* (b) *Mode II*
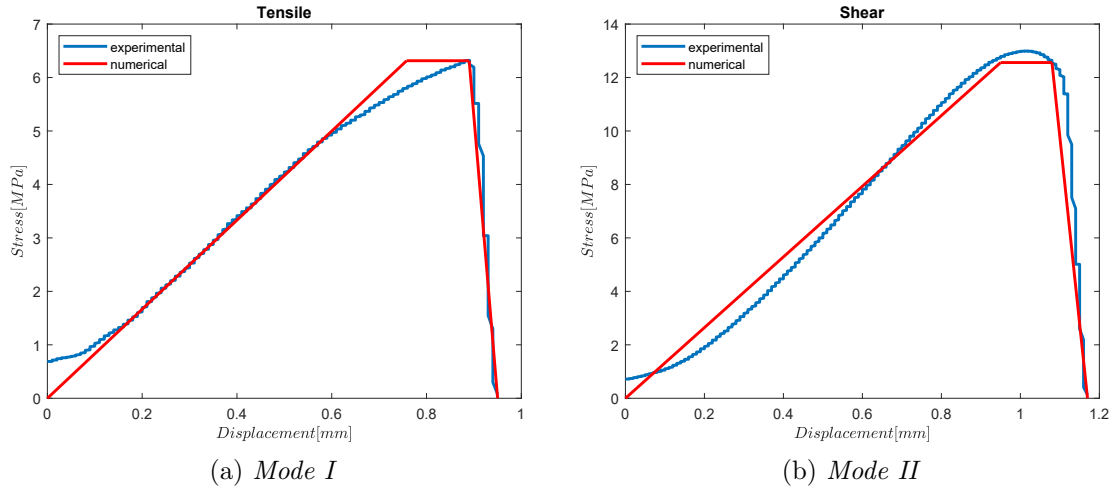
Figure 3.24: Mat_240 static traction separation law interpolation of the arcan test experimental data.

3.2 Experimental tests

The joint configurations selected for the experimental campaign were the *test A* and *test C* (cf. section §3.1.5), respectively a 20mm overlap joint with steel substrates, epoxy adhesive and a 10mm overlap with composite substrates and PU adhesive. This is the minimum number of tests necessary to evaluate all the material included in this work: epoxy and PU adhesive, DD11 steel and carbon fiber composite for the substrates. The steel substrates available for the test A were 30mm wide, with this configuration higher forces are expected but the behaviour in terms of deformation and failure mode should be unchanged (cf. section §2.2.4).

3.2.1 Specimen preparation

The substrates are beam shape parts with rectangular cross section of 30 mm x 12 mm and 20 mm x 7 mm for the steel and composite adherends respectively. They were cut with an *electric cutting machine* at the designed length. For the clamped

adherends a length of 30 mm has been taken into account for the clamping system.

The surfaces were prepared by *sandpaper grinding* with coarse grit designation P50 and refined with P150. As a last step the adherends were cleaned with acetone until no residue was left on the cloth.

Figure 3.25: DD11 substrates after surface cleaning and preparation.

For the bonding procedure the adhesive was deployed and the substrates were hand-laid according the prescribed joint configuration. With a clamping system pressure was applied for some minutes and afterwards a curing process took place in oven for 1 hour at $180°C$. Two joints were prepared for each configuration. The measured adhesive thickness was 0.6 mm for both the joint configurations.

Only quasi static tests were performed with an *Instron* machine. A 100 kN load cell was adopted and it was used a data acquisition frequency of 10 Hz. The specimen were clamped on the clamping plate and the load was applied by the crosshead with hemispherical tip. The machine configuration is shown in figure 3.27.
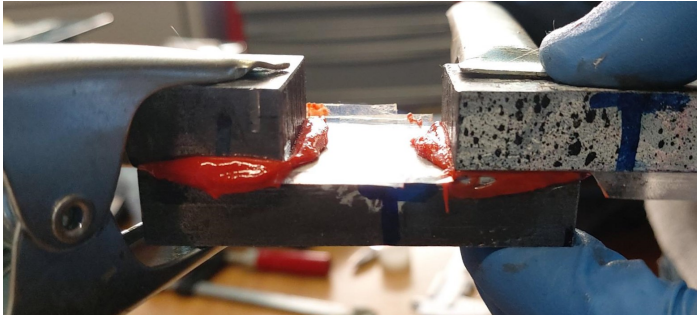
(a) *Test A*

(b) *Test C*

Figure 3.26: Bonding procedure.
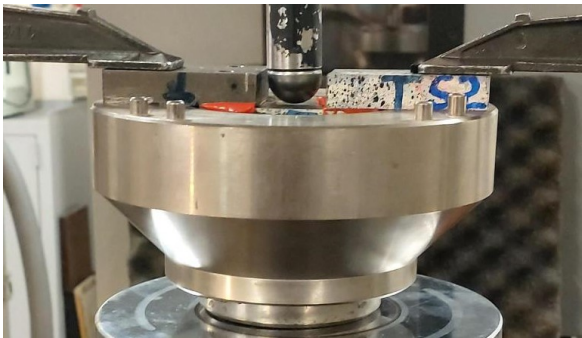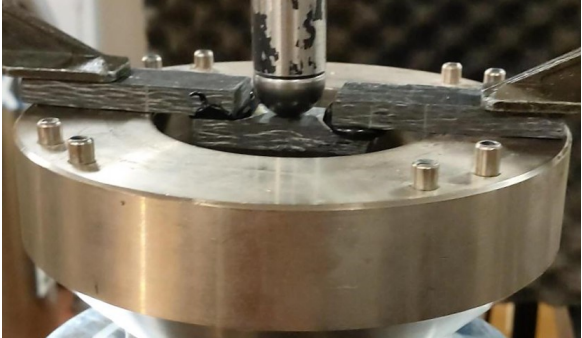
(a) *Test A* (b) *Test C*

Figure 3.27: Quasi-static test machine configuration.

3.2.2   Experimental results

The main difficulty involved in the proposed test is its need of an extreme symmetry both in geometry and materials so as to exploit an homogenous and simultaneous failure in both of the bonding regions. In all the performed tests this condition was not achieved and the failure occurred only in one of the overlaps causing the bottom adherend to slide and bend.

Between the two tested configurations the composite substrate and PU adhesive *test C* is the one that provided the better results. The data is shown in figure 3.28 and compared with the Ls-Dyna force-displacement plot of a quasi-static test. The numerical results show an almost triangular shaped graph according to the bilinear characteristic without plasticity of MAT_138. The peak load is close to the 2 *kN* that is the theoretical traction load that the adhesive can bear ($F = 2 \cdot \sigma \cdot b \cdot Ovl$). The crosshead displacement on the other hand is larger than the adhesive one due to the adherends deformation. The experimental curves are not as linear as in the numerical model in the elastic region and close to the failure exhibit a decreasing slope due to plasticity and damaging. Remarked that only one of the two overlap failed, this means that at least most of the damage is being accumulated in the failing region; once the failure occurs the load drops being the bottom adherend not clamped any more. The consequence is that not all the adhesive strength is exploited; a successful test would have continued on that trend up to higher loads but with the reported asymmetrical failure it cannot be established what its ultimate strength would have been. The PU material card that was extrapolated in previous researches interpolates quite well the elastic region and correctly reaches higher levels of force and displacement. So while the stiffness is close to the experimental results, the strength cannot be further calibrated without tests in which a failure in both the overlaps is successfully obtained.
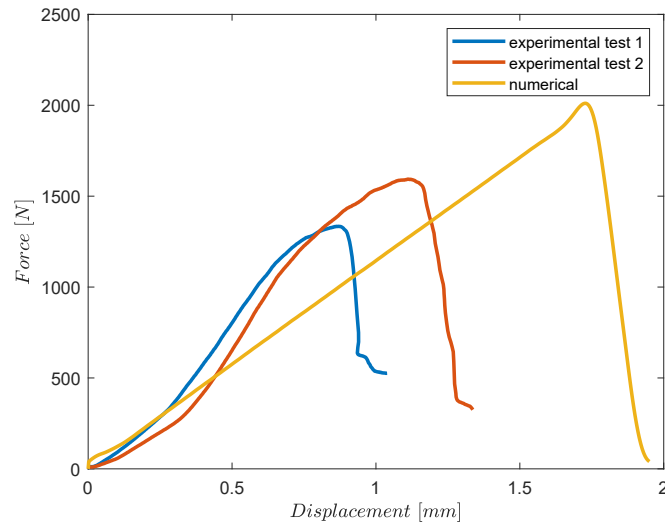
Figure 3.28: *Test C*: experimental tests force-displacement and numerical results.

In the *test A* with 20mm overlap and epoxy adhesive higher forces were expected, that together with the higher 30mm width of the substrates the clamping system was outperformed, and the specimen settled during the test causing an error in the data recorded. The results are shown in figure 3.29 and are plotted with a trend line that approximates the expected results in a successful test.

Moreover, the adhesive have been able to exploit a significantly higher strength than it was expected. The material card used in this work predicts a peak load of 8.6 *kN* that is about half of the experimental results peak, for which only one overlap regions failed. Consequently, similarly to the previous case not all the adhesive strength was exploited. It has to be remarked that the material card in 2.3 was obtained by an *arcan test* with composite substrate and 0.2 *mm* adhesive thickness. The different configuration of this test may justify the higher mechanical properties exploited. The numerical model comparison in figure 3.29 was computed with a modified material card shown in table 3.9 that better interpolates the numerical data.
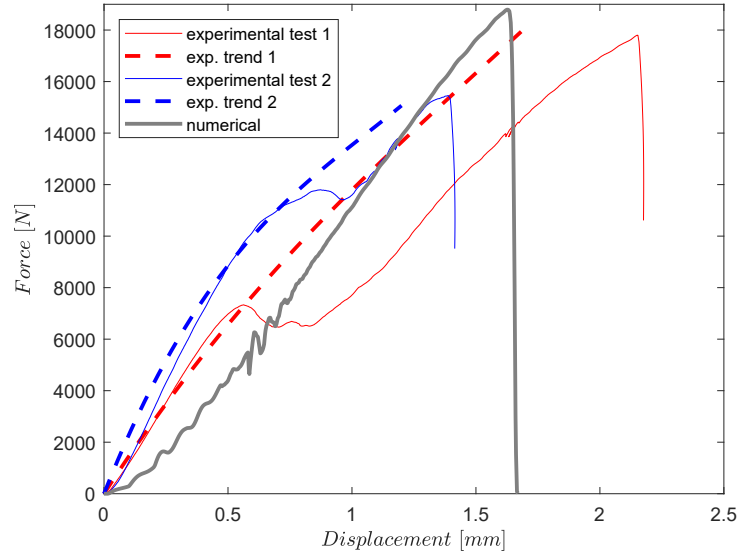
Figure 3.29: *Test A*: experimental tests force-displacement and numerical results.

Alike the previous case, also with this data it's possible to estimate only the stiffness characteristic and the correct strength of the adhesive cannot be evaluated without a simultaneous failure. This test only proved that the adhesive can reach a peel stress close to the $16MPa$ set in the FEM but further investigations are needed to understand how much room is left. Experimental evidence shows that a simultaneous failure of the adhesive would be almost unattainable, at least with a quasi-static test. A viable development would be to introduce an asymmetry in the joint to lead the failure in the weaker side or to design an alternative joint with a single overlap.

In each test a completely cohesive failure was reported, proving that with the adopted bonding procedure a good adhesion was achieved. The failed surfaces are shown in figure 3.30. It can also be observed how on the steel substrates it was reported an indent in the contact point of the crosshead, while no visible damage was present in the composite ones. Result that is well aligned with the numerical model.

*MAT_138 epoxy	
$\rho[Ton/m^3]$	1.22
$E_n[MPa]$	16.3265
$E_t[MPa]$	27.2727
GIC$[MPa \cdot mm]$	8.4
GIIC$[MPa \cdot mm]$	17.55
$\sigma_t[MPa]$	16
$\sigma_s[MPa]$	30
UND[mm]	1.05
UTD [mm]	1.17
XMU [-]	1

Table 3.9: *MAT_138 material card for epoxy adhesive calibrated on the experimental tests.

(a) *Test A (1)*   (b) *Test A (2)*

(c) *Test C (1)*   (d) *Test C (2)*
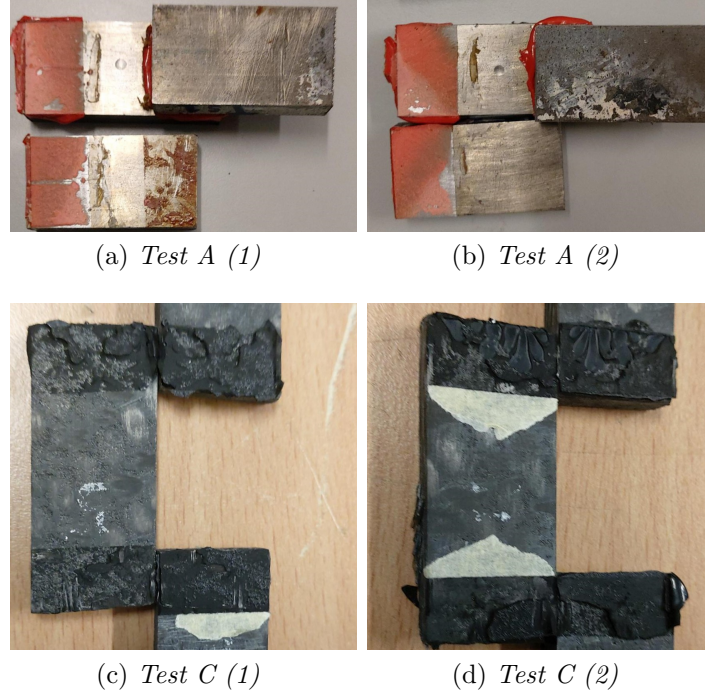
Figure 3.30: Failed specimens surfaces. A fully cohesive failure has been reported in each test.

Chapter 4

Conclusions

In this work a new model and methodology for impact tests on adhesive joints has been developed. It has been designed a *single strap lap joint* to evaluate the tensile mechanical properties of adhesives under large strain rate loading conditions. The parametrised joint geometry can be quickly adapted to a variety of material as function of the overlap length. This methodology can be a useful tool in material research as well as to finely tune the material models used in finite elements analysis. The model configuration has been designed and optimized via numerical modelling in Ls-Dyna. The simulations proved that the joint is able to to exhibit the designed tensile failure and the energy absorption capabilities of the joint have been analysed. Some experimental tests in quasi-static loading conditions have been carried out. The tests revealed the main weakness of the proposed joint: in order to evaluate the mechanical properties of the coupled materials a simultaneous failure in both the overlap regions is needed to occur. Consequently an acceptable failure would be achieved only with a very accurate bonding procedure and this condition is unlikely to be obtained without a dedicated jig that can guarantee a good alignment. The main future development would be to implement some dynamic tests that would assess the actual behaviour of the model under large strain rate.

List of Figures

Bibliography

[1] ISO 11003-2. *Adhesives – Determination of shear behaviour of structural adhesives*. 2019.

[2] ISO 11343:2019. *Adhesives – Determination of dynamic resistance to cleavage of high-strength adhesive bonds under impact wedge conditions - Wedge impact method*. 2019.

[3] ISO 25217:2009. *Adhesives – Determination of the mode 1 adhesive fracture energy of structural adhesive joints using double cantilever beam and tapered double cantileveer bram specimens*. 2009.

[4] ISO 9653. *Adhesives – Test method for shear strength of adhesive bonds*. 1998.

[5] A. Beevers and M.D. Ellis. "Impact behaviour of bonded mild steel lap joints". In: *International Journal of Adhesion and Adhesives* 4.1 (1984). Special Issue Adhesives in Land Transport, pp. 13–16. ISSN: 0143-7496. DOI: `https://doi.org/10.1016/0143-7496(84)90055-1`. URL: `http://www.sciencedirect.com/science/article/pii/0143749684900551`.

[6] B.R.K. Blackman et al. "The fracture behaviour of structural adhesives under high rates of testing". In: *Engineering Fracture Mechanics* 76.18 (2009), pp. 2868–2889.

[7] Georges CHALLITA and Ramzi Othman. "Finite-element analysis of SHPB tests on double-lap adhesive joints". In: *International Journal of Adhesion and Adhesives* 30.4 (2010), pp. 236–244. DOI: `10.1016/j.ijadhadh.2010.02.004`. URL: `https://hal.archives-ouvertes.fr/hal-01006902`.

[8] J.F. Lancaster. "3 - The use of adhesives for making structural joints". In: *Metallurgy of Welding (Sixth Edition)*. Ed. by J.F. Lancaster. Sixth Edition. Woodhead Publishing Series in Welding and Other Joining Technologies. Woodhead Publishing, 1999, pp. 54–84. ISBN: 978-1-85573-428-9. DOI: `https://doi.org/10.1533/9781845694869.54`. URL: `http://www.sciencedirect.com/science/article/pii/B9781855734289500050`.

[9] Lijuan Liao et al. "3-D FEM stress analysis and strength evaluation of single-lap adhesive joints subjected to impact tensile loads". In: *International Journal of Adhesion and Adhesives - INT J ADHES ADHES* 31 (Oct. 2011), pp. 612–619. DOI: `10.1016/j.ijadhadh.2011.06.008`.

[10]   J. J. M. Machado, E. A. S. Marques, and Lucas F. M. da Silva. "Adhesives and adhesive joints under impact loadings: An overview". In: *The Journal of Adhesion* 94.6 (2018), pp. 421–452.

[11]   Lucas F.M. da Silva (Editor) et al. *Testing Adhesive Joints: Best Practices.* Weinheim: Wiley-VCH Verlag Co, 2012.

[12]   Uday K. Vaidya et al. "Experimental-numerical studies of transverse impact response of adhesively bonded lap joints in composite structures". In: *International Journal of Adhesion and Adhesives* 26.3 (2006), pp. 184–198.